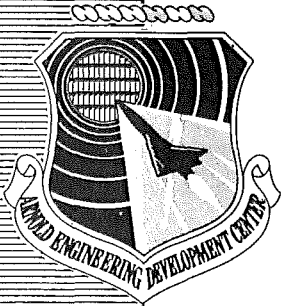


copy 14



EVALUATION OF AN AIRJET DISTORTION GENERATOR USED TO PRODUCE STEADY-STATE, TOTAL-PRESSURE DISTORTION AT THE INLET OF TURBINE ENGINES

ENGINE TEST FACILITY
ARNOLD ENGINEERING DEVELOPMENT CENTER
AIR FORCE SYSTEMS COMMAND
ARNOLD AIR FORCE STATION, TENNESSEE 37389

December 1976

Final Report for Period October 16, 1975 to February 4, 1976

Approved for public release; distribution unlimited.

TECHNICAL REPORTS
FILE COPY

PROPERTY OF U.S. AIR FORCE
AEDC TECHNICAL LIBRARY

Prepared for

DIRECTORATE OF TECHNOLOGY (DY)
ARNOLD ENGINEERING DEVELOPMENT CENTER
ARNOLD AIR FORCE STATION, TENNESSEE 37389

NOTICES

When U. S. Government drawings specifications, or other data are used for any purpose other than a definitely related Government procurement operation, the Government thereby incurs no responsibility nor any obligation whatsoever, and the fact that the Government may have formulated, furnished, or in any way supplied the said drawings, specifications, or other data, is not to be regarded by implication or otherwise, or in any manner licensing the holder or any other person or corporation, or conveying any rights or permission to manufacture, use, or sell any patented invention that may in any way be related thereto.

Qualified users may obtain copies of this report from the Defense Documentation Center.

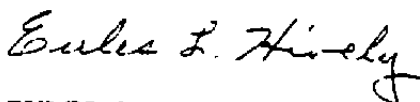
References to named commercial products in this report are not to be considered in any sense as an endorsement of the product by the United States Air Force or the Government.

This report has been reviewed by the Information Office (OI) and is releasable to the National Technical Information Service (NTIS). At NTIS, it will be available to the general public, including foreign nations.

APPROVAL STATEMENT

This technical report has been reviewed and is approved for publication.

FOR THE COMMANDER



EULES L. HIVELY
Research and Development
Division
Directorate of Technology



ROBERT O. DIETZ
Director of Technology

UNCLASSIFIED

REPORT DOCUMENTATION PAGE		READ INSTRUCTIONS BEFORE COMPLETING FORM
1 REPORT NUMBER AEDC-TR-76-141	2 GOVT ACCESSION NO.	3 RECIPIENT'S CATALOG NUMBER
4 TITLE (and Subtitle) EVALUATION OF AN AIRJET DISTORTION GENERATOR USED TO PRODUCE STEADY-STATE, TOTAL-PRESSURE DISTORTION AT THE INLET OF TURBINE ENGINES	5 TYPE OF REPORT & PERIOD COVERED Final Report-October 16, 1975 to February 4, 1976	
	6 PERFORMING ORG REPORT NUMBER	
7 AUTHOR(s) B. W. Overall, ARO, Inc.	8 CONTRACT OR GRANT NUMBER(s)	
9 PERFORMING ORGANIZATION NAME AND ADDRESS Arnold Engineering Development Center (DY) Air Force Systems Command Arnold Air Force Station, Tennessee 37389	10 PROGRAM ELEMENT, PROJECT, TASK AREA & WORK UNIT NUMBERS Program Element 65807F	
11 CONTROLLING OFFICE NAME AND ADDRESS Arnold Engineering Development Center (DYFS) Arnold Air Force Station, Tennessee 37389	12 REPORT DATE December 1976	
	13 NUMBER OF PAGES 81	
14 MONITORING AGENCY NAME & ADDRESS (if different from Controlling Office)	15 SECURITY CLASS (of this report) UNCLASSIFIED	
	15a DECLASSIFICATION/DOWNGRADING SCHEDULE N/A	
16 DISTRIBUTION STATEMENT (of this Report) Approved for public release; distribution unlimited.		
17 DISTRIBUTION STATEMENT (of the abstract entered in Block 20, if different from Report) <i>1. Turbofan engines -- TF30-P-3</i> <i>2. air inlets -- Distortion</i> <i>3. Distortion</i>		
18 SUPPLEMENTARY NOTES <i>4. Distortion generators</i> Available in DDC		
19 KEY WORDS (Continue on reverse side if necessary and identify by block number) performance pressure (total) turbofan engine testing distortion airjet generator steady state TF30-P-3		
20 ABSTRACT (Continue on reverse side if necessary and identify by block number) A performance evaluation of an airjet distortion generator system used to produce steady-state, total-pressure distortion at the inlet to a turbine engine was conducted. The capability of the system to duplicate screen-generated, parametric distortion patterns (180 deg, one per revolution; tip radial; hub radial) and to maintain a constant composite distortion pattern over a range of airflows is presented. A comparison of the effects of inlet		

UNCLASSIFIED

UNCLASSIFIED

20. ABSTRACT (Continued)

distortion produced by screens to that produced by the airjet distortion generator system on the stability characteristics of a present-day turbofan engine is described.

UNCLASSIFIED

PREFACE

The work reported herein was conducted by the Arnold Engineering Development Center (AEDC), Air Force Systems Command (AFSC), under Program Element 65807F. The results of the test were obtained by ARO, Inc. (a subsidiary of Sverdrup Corporation), contract operator of AEDC, AFSC, Arnold Air Force Station, Tennessee, under ARO Project Number R41D-07A. Data analysis and reporting were conducted under ARO Project Number R32P-A4A. The author of this report was B. W. Overall, ARO, Inc. The data analysis was completed on April 4, 1976, and the manuscript (ARO Control No. ARO-ETF-TR-76-91) was submitted for publication on August 17, 1976.

CONTENTS

	<u>Page</u>
1.0 INTRODUCTION	7
2.0 APPARATUS	
2.1 Test Article	8
2.2 Test Equipment	11
2.3 Installation	12
2.4 Instrumentation	13
2.5 Calibration	14
3.0 PROCEDURE	
3.1 Simulated Flight Condition	15
3.2 Airjet Distortion Generator System	15
3.3 Engine Surge Testing	16
3.4 Methods of Calculation	16
4.0 RESULTS AND DISCUSSION	
4.1 Inlet Total-Pressure Pattern Fidelity	17
4.2 Compression System Components Total- Pressure and Temperature Profiles	20
4.3 Engine Stability Response	20
4.4 Evaluation of Differences between Screens and the AJDG as Distortion Systems	23
5.0 SUMMARY OF RESULTS	25
REFERENCES	27

ILLUSTRATIONS

Figure

1. Functional Schematic of the Airjet Distortion Generator System	29
2. Airjet Distortion Generator Strut Details	
a. Installation in Engine Air Supply Duct	30
b. Dimensional Schematic	31
3. Functional Schematic of the Airjet Distortion Generator Airflow Distribution Control System	32
4. Computer Control Logic for Airjet Distortion Generator Airflow Distribution System	33
5. Airjet Distortion Generator/Engine Installation in Altitude Test Cell	34
6. Engine Inlet Duct Configuration Details	
a. Distortion Screen Installed	35
b. Airjet Distortion Generator Struts Installed	36

<u>Figure</u>	<u>Page</u>
7. Airjet Distortion Generator Air Supply System Instrument Locations	37
8. Engine Instrument Station Locations	38
9. Instrumentation Details, Looking Upstream	
a. Engine Inlet Duct	39
b. Engine	40
10. Engine Inlet Isobar Maps for Screen and Airjet Distortion	
a. 180-deg Pattern, WA2R2 = 200 lbm/sec	41
b. 180-deg Pattern, WA2R2 = 170 lbm/sec	42
c. Tip Radial Pattern, WA2R2 = 200 lbm/sec	43
d. Tip Radial Pattern, WA2R2 = 170 lbm/sec	44
e. Hub Radial Pattern, WA2R2 = 200 lbm/sec	45
f. Hub Radial Pattern, WA2R2 = 170 lbm/sec	46
11. Engine Inlet Isobar Maps for the Airjet Distortion Generator-Produced Composite Pattern	47
12. Relative Time Requirements to Produce a Specified Distortion Pattern with Screens and with the Airjet Distortion Generator System	48
13. Power Spectral Density Characteristics for the 180-deg Distortion Pattern	
a. WA2R2 = 200 lbm/sec	49
b. WA2R2 = 170 lbm/sec	49
14. Power Spectral Density Characteristics for the Tip Radial Distortion Pattern	
a. WA2R2 = 200 lbm/sec	50
b. WA2R2 = 170 lbm/sec	50
15. Power Spectral Density Characteristics for the Hub Radial Distortion Pattern	
a. WA2R2 = 200 lbm/sec	51
b. WA2R2 = 170 lbm/sec	51
16. Effects of Primary and Secondary Air Temperature Mismatch on Engine Inlet Temperature	52
17. Comparison of Compression Component Total-Pressure Profiles with Screen and with Airjet Distortion Generator Hub Radial Distortion	53

<u>Figure</u>		<u>Page</u>
18.	Comparison of Compression Component Total-Temperature Profiles with Screen and with Airjet Distortion Generator Hub Radial Distortion	54
19.	Effects of Simultaneous Loading of Low- and High-Pressure Compressors on Engine Match, Undistorted Inlet	55
20.	Compressor Performance with Undistorted Engine Inlet, 45,000 ft, Mach No. 1.2	56
21.	Comparison of High-Pressure Compressor Performance with Screen and with Airjet Distortion Generator 180-deg Engine Inlet Distortion Pattern, 45,000 ft, Mach No. 1.2.	57
22.	Comparison of Low-Pressure Compressor Performance with Screen and with Airjet Distortion Generator Tip Radial Engine Inlet Distortion Pattern, 45,000 ft, Mach No. 1.2	58
23.	Comparison of High-Pressure Compressor Performance with Screen and with Airjet Distortion Generator Hub Radial Engine Inlet Distortion Pattern, 45,000 ft, Mach No. 1.2	59
24.	Schematic Representation of the Dynamic Flow Field Existing with Airjet Distortion Generator Hub Radial Distortion Patterns	
	a. Low Secondary Airflow	60
	b. Intermediate Secondary Airflow	60
	c. High Secondary Airflow	60
25.	Comparison of Radial Distribution of Total-Pressure Loss with Screen and Airjet Distortion Generator Hub Radial Pattern at a Corrected Engine Airflow of 200 lbm/sec. .	61

TABLES

1.	Posttest Estimates of Data Uncertainties	62
2.	Summary of Steady-State Inlet Pattern Quality with Airjet Distortion Generator	65

APPENDIX

	<u>Page</u>
A. METHODS OF CALCULATION	67
NOMENCLATURE	79

1.0 INTRODUCTION

The recent increase of emphasis on the effects of inlet total-pressure distortion on turbine engine stability and performance has resulted in a major effort at ground test facilities to improve the duplication of the inlet total-pressure profiles encountered during operation of engines over the aircraft flight envelope. An engine will encounter a variety of distortion patterns over a wide range of engine airflow rates. In order to adequately define the engine stability characteristics, testing with a large number of unique distortion patterns is required. The most widely accepted approach to producing the distortion patterns has been the use of complex assemblies of various porosity screens. The inherent inflexibility of the screen configuration (single design operating point) and the extensive development effort required for each screen dictated the need for a more flexible method of producing total-pressure distortion. In response to this need, an effort to provide an alternate method has been in progress at the Arnold Engineering Development Center (AEDC) during recent years (Refs. 1 and 2).

The airjet distortion generator (AJDG) system is a method for producing steady-state, total-pressure spatial distortion at the inlet to a turbine engine. The airjet system produces steady-state distortion by injecting secondary air counter to the primary airflow. By injecting a controlled amount of secondary airflow in specific spatial locations, a wide range of inlet distortion patterns can be produced. Digital computer control of secondary airflow provides a dial-a-pattern capability that makes the airjet system a highly flexible and efficient test tool.

The development of the AJDG system at the AEDC has progressed through the stages of feasibility demonstration, functional and structural evaluation of the air distribution system, and evaluation of the air temperature-conditioning system. A feasibility demonstration of the airjet system concept was conducted under the sponsorship of the Air Force Aeropropulsion Laboratory (AFAPL) during stability test evaluation of a TF30-P-3 turbofan engine (Ref. 1). A subsequent functional and structural evaluation of the airjet system, also sponsored by the AFAPL, is reported in Ref. 2. An evaluation of the airjet system air supply pressure- and temperature-conditioning system was sponsored by and conducted at the AEDC. The results of these

prior investigations indicated that the airjet system was a viable method for producing steady-state, total-pressure distortion.

The purpose of the investigation reported herein was to validate the capability of the total system when utilized forward of a typical, present-day turbofan engine in a normal turbine engine test environment. The specific test objectives were (1) to assess the fidelity with which the airjet system could produce a desired parametric total-pressure pattern, (2) to demonstrate the capability of the airjet system to maintain a composite total-pressure pattern over a range of engine airflow rates, and (3) to compare the effects of inlet distortion produced by screens to those produced by the airjet distortion generator system on the stability characteristics of a present-day turbofan engine.

This report defines the fidelity of parametric inlet pressure distortion patterns produced by the airjet system and describes the capability of the airjet system to maintain a composite distortion pattern over a range of engine power settings. A comparison of the stability sensitivity of a present-day turbofan engine with screen-produced distortion to that with airjet-produced distortion is presented. Operational characteristics of the airjet system are discussed.

2.0 APPARATUS

2.1 TEST ARTICLE

The airjet distortion generator is a system used to produce steady-state, total-pressure distortion at the inlet of a turbine engine by forward injection of secondary air (counter to the primary air) at selected spatial locations. The AJDG system consists of two basic subsystems, an air supply temperature- and pressure-conditioning system and an airflow distribution system.

The air supply temperature- and pressure-conditioning system conditions the secondary air to the temperature level required to match the primary engine inlet air temperature and throttles the secondary airflow to produce a desired pressure level at the supply manifold.

The airflow distribution system meters secondary airflow to each of the 56 injection ports as required to produce the

desired total-pressure decrement at each spatial location. A functional schematic of the AJDG system is presented in Fig. 1.

2.1.1 Air Supply Temperature- and Pressure-Conditioning System

The AJDG air supply temperature- and pressure-conditioning system is comprised of the basic subsystems listed below:

1. High-pressure (3,000 psia) air supply, flow-rate measurement and control stations,
2. High-temperature (above ambient) air-conditioning system,
3. Low-temperature air-conditioning system (not active during the tests reported herein),
4. Conditioned air manifold assembly, and
5. Steam and nitrogen service systems.

The filtered high-pressure air supply pressure is regulated by a control valve upstream of a dual-range flow-measuring station. Airflow through either or both of the flow-measuring stations is controlled by remotely operated on/off valves. The flow-measuring system consists of a parallel leg arrangement with ASME sharp-edged orifices sized to accommodate specific airflow ranges (5 to 20 and 16 to 40 lbm/sec). Air discharged from the flow-measuring station is directed through either the high- or low-temperature-conditioning system.

The high-temperature air-conditioning system consists of an airflow leg through a steam heat exchanger and a bypass airflow leg. Desired air temperature at the outlet of the high-temperature air-conditioning system is attained by mixing "hot air" from the heat exchanger with ambient supply air. Airflow split through the two legs is regulated by the position of control valves in each leg.

The low-temperature air-conditioning system, although not active for the test reported herein, operates in the same manner as the high-temperature-conditioning system.

An engine inlet bypass capability is provided in order to independently operate the AJDG system (during system startup and shutdown) while the desired temperature and flow rate is being established.

2.1.2 Secondary Airflow Distribution System

Conditioned air is directed from the manifold to the desired spatial location and counter to the direction of primary airstream flow using a set of 56 metering valves, connecting tubing, and drilled passage struts (Fig. 2). The metering valves regulate the flow rate through each strut passage (spatial location) as required for the specific total-pressure decrement required in that location. Manifold pressure is maintained at a level which ensures that each strut discharge port operates as a sonic orifice. The struts are aerodynamically designed such that the strut body produces minimum disturbance to the primary airstream.

The airjet valves are individually controlled by a digital computer. A functional schematic of the airflow distribution system control is presented in Fig. 3. Engine inlet pressure level is determined from total-pressure measurements at the engine face. The pressure levels measured at the engine inlet are transposed to equivalent locations (comparable flow area for each pressure value) at the plane of the jets and normalized by the face average pressure. The transposed local pressure ratios are interpolated to the locations of the 56 jets. Circumferential interpolation is linear, whereas radial interpolation is from a second-order Lagrangian curve fit. The computer compares the actual pressure level at each spatial location to the desired level and commands the airjet valves to either open or close as required to establish the desired pressure levels.

The command to each individual airjet valve is determined by the digital computer program logic as shown in Fig. 4. Basic logic functions determine the overall pattern root mean square error (RMSE) and the individual error (EI) at each spatial location. Valve direction is determined by comparing the measured pressure level (PRMI) with the desired pressure level (PRDI) at each spatial location; if the measured pressure level is higher than desired, the valve is directed to open; if measured pressure is lower than desired, the valve is directed to close. The selection of control valves to be repositioned is determined by comparing the error in local pressure level with the overall pattern error. Those valves controlling secondary airflow to areas with local pressure errors greater than the overall pattern error are directed to move and all remaining valves are unchanged. The amount of valve movement is the same for all valves and is determined by comparing the

overall pattern error with preselected ranges. The range of overall pattern error dictates the particular valve travel time. Valve travel times are selected such that valve travel becomes smaller as overall pattern error is reduced.

Valve command control logic is summarized as follows:

Valve Selection

$EI > RMSE$
Move

$EI \leq RMSE$
No Movement

Valve Direction

$(PRDI-PRMI) > 0$
Close

$(PRDI-PRMI) \leq 0$
Open

Valve Travel

$RMSE > X$
Timer #1

$X \geq RMSE \geq Y$
Timer #2

$RMSE < Y$
Timer #3

2.2 TEST EQUIPMENT

2.2.1 Turbofan Engine

The engine used for this test is a production model, present-day turbofan engine. The engine is a low bypass, nonaugmented turbofan engine of the 15,000-lbf-thrust class.

For this test the engine was operated in the production configuration except that a facility high-pressure air supply system was installed to inbleed air to the high-pressure compressor (HPC) discharge to back-pressure the high-pressure compressor and an exhaust nozzle plug was installed to vary the nozzle exit area and back-pressure the fan.

2.2.2 Inlet Distortion Screens

Three distortion screen patterns were used during the test program. The desired total-pressure patterns which were duplicated by the AJDG were defined from measured inlet pressure values with the screens installed. Three screen patterns were used to simulate the following inlet distortion patterns:

Screen ConfigurationPattern

R41D-07A-1F	180 deg, one per revolution
R41D-07A-2F	Tip radial
R41D-07A-3F	Hub radial

Each screen configuration was comprised of a single, constant porosity wire cloth. The screen was permanently mounted on a 1- by 1- by 0.125-in. stainless steel backing grid.

2.3 INSTALLATION

The airjet distortion generator system was used in conjunction with a normal engine test installation. A schematic of the overall test installation is presented in Fig. 5.

The initial distortion testing was with distortion screens (airjet struts not installed). The screens were installed at the same relative location as the airjet struts (Fig. 6).

The AJDG supply air pressure- and temperature-conditioning system was located in the test area adjacent to the Engine Test Facility (ETF) Propulsion Development Test Cell (T-4). A 4-in.-diam supply line connected the high-pressure air supply to the AJDG conditioning system. The AJDG manifold was mounted in the forward end of the test cell. A 4-in.-diam line connected the AJDG conditioning system and the manifold.

The airjet struts were installed in the engine inlet duct approximately 42 in. upstream of the engine inlet plane (Fig. 6b). A 3/4-in. airflow control valve was installed at each of the manifold discharge ports. Stainless steel, 3/4-in.-diam tubing connected each control valve to its appropriate strut passage.

The engine assembly and engine support mount were installed on a thrust stand which was flexure mounted on a model support cart. The primary airflow rate was measured using a critical-flow venturi located approximately 45 ft upstream of the engine bellmouth. The engine inlet plenum contained a flow-straightening grid with uniform screen overlay, a core blockage plate, and a bellmouth to ensure a uniform low distortion airflow into the engine inlet duct.

The engine inlet ducting, attached to the instrumented engine inlet extension, extended into a zero-leakage, labyrinth-type air seal.

An exhaust gas ejector, mounted approximately 16 in. downstream of the exhaust nozzle, utilized the energy of the engine exhaust to augment the facility exhaust machines. A high-pressure compressor inbleed air system and a movable exhaust nozzle plug were installed to load the engine compression system during stability testing.

A detailed description of Test Cell T-4 is presented in Ref. 3.

2.4 INSTRUMENTATION

Instrumentation was provided to measure aerodynamic pressures and temperatures as required to monitor the operation of the airjet distortion generator system. Airjet supply system aerodynamic pressure and temperature sensors were located as shown in Fig. 7.

Engine instrumentation was provided to measure aerodynamic pressures and temperatures, rotor speeds, and other engine parameters as required for proper and safe operation. Aerodynamic pressure and temperature sensors were located at the stations shown in Fig. 8. Diagrams showing the number and type of instrumentation at each station are presented in Fig. 9.

Aerodynamic pressures were measured with strain-gage-type transducers. Temperatures were measured with iron-constantan, copper-constantan, and Chromel®-Alumel® thermocouples. The voltage outputs of the transducers and thermocouples were recorded on magnetic tape from high-speed, analog-to-digital converters and converted to engineering units by an electronic digital computer. Selected channels of pressure and temperature were displayed in the control room for observation during engine operation.

Dynamic pressure measurements were obtained at the engine inlet, fan exit, intermediate compressor exit, and high-pressure compressor exit using semiconductor strain-gage transducers and associated electronic circuitry. The analog outputs of the transducers were recorded on magnetic tape.

Power lever and high-pressure compressor inlet guide vane positions were obtained using linear potentiometers

connected to the actuation linkages. The voltage outputs of the potentiometers were recorded on magnetic tape from high-speed analog-to-digital converters and converted to engineering units by a digital computer. Voltage outputs from each potentiometer were used to drive a milliammeter display in the control room.

Fan and high-pressure compressor rotor speeds were measured using variable reluctance tachometer generators. The output signals were recorded on magnetic tape from the frequency-to-analog converter and converted to rpm by a digital computer. Control room indication was displayed on a digital frequency counter and also on a milliammeter display from a frequency-to-analog converter.

The instrumentation ranges, recording methods, and posttest estimates of measurement uncertainty are presented in Table 1.

2.5 CALIBRATION

All transducer and system calibrations performed during the test are traceable to the National Bureau of Standards (NBS). Each link in the traceability chain back to the NBS is maintained and documented by the AEDC Standards Laboratory (Ref. 4).

The aerodynamic pressure measurement transducers utilized in the Automatic Multiple Pressure Scanning (AMPS) System (Table 1) were in-place calibrated before and after each test period by applying multiple pressure levels within the pressure range from 0.5 to 50 psia. Each applied pressure level was measured with a pressure-measuring device calibrated in the AEDC Standards Laboratory. The AMPS System transducers utilized for aerodynamic pressure measurements above 50 psia, and all other pressure transducers (Table 1), were calibrated in the AEDC Standards Laboratory to establish their applied pressure versus resistance shunt equivalent pressure relationship. Before and after each test period, multiple step resistance shunt calibrations were performed to calibrate the pressure-recording system. For example, a 100-psia pressure transducer in the AMPS system was in-place calibrated up to 50 psia and resistance shunt calibrated from 50 to 100 psia.

All facility-supplied thermocouples were fabricated from wire conforming to Instrument Society of America specifications. Internal engine thermocouples were supplied

by the engine manufacturer. Before and after each test period, known millivolt levels were applied to each temperature-recording system, and the corresponding temperature equivalents were obtained from 150°F reference tables based on the NBS temperature versus millivolt tables. Nonlinearity in the thermocouple characteristics were accounted for in the data reduction program.

The position indicators for power lever position and high-pressure compressor guide vane angle were in-place calibrated at selected intervals during the test program. End point calibrations were made based on mechanical stops built into the engine hardware.

The speed-measuring system transducer and transducer-to-engine rotor coupling characteristics were utilized to determine the rotor revolutions per minute versus frequency relationship. Before and after each test period, the speed-recording systems were calibrated by applying known frequency input levels from a frequency generator calibrated in the AEDC Standards Laboratory.

3.0 PROCEDURE

3.1 SIMULATED FLIGHT CONDITION

Conditioned air was supplied to the engine inlet at the total pressure and temperature required to simulate the desired flight condition. Test cell pressure was set at the level corresponding to the desired altitude in geopotential feet, based on 1962 U. S. Standard Atmosphere (Ref. 5). One-dimensional, isentropic, compressible flow functions were used to determine the free-stream total temperature and pressure for the desired Mach number. An engine inlet pressure ram recovery, as defined in Ref. 6, was used to determine the desired compressor inlet total pressure for all flight conditions.

All testing was conducted at a simulated flight condition corresponding to 45,000 ft, Mach number 1.2, hot day condition.

3.2 AIRJET DISTORTION GENERATOR SYSTEM

The airjet distortion generator system was brought online by flowing secondary air through the bypass system.

The system was set to operate near the secondary airflow expected to be required to produce the specified inlet distortion. Air supply system automatic controls were set to deliver secondary air conditioned to the temperature level of the primary air at a pressure level of approximately 450 psia at the manifold. At the time inlet distortion was required, the secondary air distribution system computer control program was activated. As the airjet distribution system valves were opened, the secondary air was diverted to the engine inlet by closing the bypass valves.

3.3 ENGINE SURGE TESTING

Basic engine operation for surge testing was the same for all inlet conditions (clean, airjet distortion, and screen distortion). The engine was stabilized on its normal operating line at the selected power setting. Then the engine was driven from its normal operating line to surge using inbleed air to the high compressor discharge and a movable plug to vary exhaust nozzle area. Engine airflow was maintained constant by adjusting the power lever (resulting in a slight increase in rotor speed match).

3.4 METHODS OF CALCULATION

The methods used to calculate the data parameters are presented in Appendix A.

4.0 RESULTS AND DISCUSSION

A performance evaluation of an airjet distortion generator system was conducted with three parametric and one composite total-pressure distortion pattern. The compression system stability characteristics of a present-day turbofan engine with screen-produced, inlet total-pressure distortion are compared to stability characteristics with airjet distortion generator-produced distortion for each of the three parametric distortion patterns.

The primary objectives of the test were to assess the fidelity of the total-pressure distortion patterns produced by the airjet system, to determine the ability of the airjet system to maintain a specified composite distortion pattern over a range of airflow rates, and to evaluate any differences in engine stability with screen and airjet-produced distortion.

The test results relative to primary objectives are presented herein. Additional test results concerning airjet system operation are included.

4.1 INLET TOTAL-PRESSURE PATTERN FIDELITY

The AJDG system is designed to produce steady-state, total-pressure spatial distortion at the inlet of a turbine engine. The secondary airflow introduced by the AJDG system is conditioned to match the primary engine supply air temperature. The fidelity of the inlet distortion pattern produced by the AJDG system was evaluated for three parametric inlet distortion patterns (180 deg, one per revolution; tip radial; hub radial). Each pattern was first produced and measured using a distortion screen installed in the engine inlet ducting. The AJDG system was then used to reproduce the inlet pressure pattern measured with the screen installed.

4.1.1 Steady-State, Total-Pressure Distortion

Steady-state, total-pressure distortion pattern quality can be described by the pattern characteristic appearance and distortion level, P2DIST (Appendix A). Pattern characteristics, as shown by isobar maps at the engine inlet, are presented in Fig. 10. For each pattern, the AJDG system produced similar areas of high and low total pressure and maintained similar area contours to those produced by the distortion screens. The distortion level of each pattern produced by the AJDG system agreed with the screen-produced distortion level within three-percent absolute distortion.

Although pattern characteristics and distortion level are good indications of pattern quality, the specific definition of each inlet pattern should be made on the basis of a comparison of individual pressure levels at the specific spatial locations. Individual pressure values for each pattern are compared in Fig. 10.

The overall agreement between the measured and desired local pressure levels can be quantified by the RMSE (Appendix A). For the three patterns, the RMSE ranged from ± 0.7 to ± 2.3 percent. The largest RMSE generally occurred at the highest distortion levels. A summary of RMSE values for all patterns is presented in Table 2.

4.1.2 Inlet Total-Pressure Pattern Repeatability

The high degree of flexibility associated with the AJDG system was demonstrated for a typical composite pressure distortion pattern encountered during aircraft flight maneuver. A distortion pattern measured during a flight test program with 48 total-pressure probes at the engine inlet was used as a desired pattern. This pattern was defined by the 48 total-pressure values located at the center of equal areas. The capability of the AJDG system to produce a constant composite distortion pattern over a range of corrected engine airflows from 160 to 240 lbm/sec (idle to intermediate engine power at 45,000 ft, Mach No. 1.2 condition) is demonstrated by the isobar maps of the pattern presented in Fig. 11. At each airflow level, the pattern characteristics were reproduced with the distortion level (P2DIST) maintained within the range from 11 to 15 percent as airflow was increased from 160 to 240 lbm/sec. Overall pattern quality was excellent with RMSE ranging from 1.0 to 1.4 percent (Table 2).

4.1.3 Steady-State, Total-Pressure Set Time

An advantage of the AJDG system is the capability to rapidly set a desired distortion pattern upon command. The system is capable of changing the engine inlet conditions from clean (low distortion) to a specified distortion pattern or from one distortion pattern to another during a given test period, whereas screen-generated distortion testing is limited to a single distortion pattern at the design engine airflow level during a given test period. The time savings associated with the AJDG system includes both engine test time and the time required to design, fabricate, install, and calibrate a distortion screen. A comparison of the time required to produce a specific distortion pattern with screens and with the AJDG system is shown in Fig. 12. The total time required to develop a distortion screen with an acceptable pattern quality (RMSE approximately 2 percent) is on the order of 12 working days. With the AJDG system, a specific, desired distortion pattern is available essentially upon command; the typical time required for the AJDG system to set a desired pattern has been demonstrated to be less than two minutes.

4.1.4 Time Variant Inlet Total Pressure

A limited survey of time variant total-pressure levels was made in the inlet airstream upstream of the engine face. The measurements (two spatial locations, Fig. 9a) were sufficient to provide only a qualitative assessment of the

time variant pressure characteristics at the engine face of the engine inlet. A comparison of the power spectral density functions for the inlet total pressure is presented in Figs. 13 through 15 for both AJDG and screen-produced distortion patterns. Inlet turbulence ($\Delta PRMS/P2$, Appendix A) was consistently higher with the AJDG system than with screens. Inlet turbulence levels were calculated for the frequency range from the lower measuring limit (5 Hz) to the frequency level corresponding to the fan rotor speed (160 Hz). Local turbulence levels for the screen-produced distortion patterns were on the order of one percent. With the AJDG system, the local turbulence levels, at corrected engine airflows of 200 lbm/sec, were two, three, and five percent for the 180 deg, tip radial, and hub radial patterns, respectively. The increase in turbulence levels for the AJDG-produced distortion patterns over those levels for screen-produced patterns is indicative of differences in the inlet flow field as discussed in Section 4.4.

4.1.5 Steady-State, Inlet Total-Temperature Match Capability

Testing of the AJDG system with the engine installed was conducted using secondary air that was temperature conditioned to match the primary engine supply air temperature within $\pm 3^\circ\text{F}$. In addition, an evaluation of the inlet temperature error (difference in measured temperatures downstream of flowing jets and nonflowing jets) resulting from primary and secondary air mixing was conducted during testing with an engine inlet simulator. In this evaluation, the primary and secondary air temperatures were intentionally mismatched in selected increments up to 15°F at various levels of secondary airflow. Engine inlet temperature error as a function of primary and secondary air temperature mismatch is presented in Fig. 16. At temperature mismatch levels up to 3°F , no error in inlet temperature was discernible. An inlet temperature error of approximately 0.5°F was evident at a primary and secondary air temperature mismatch of 6°F . For a temperature mismatch of up to 6°F , there is no defined trend of temperature error with secondary airflow. At a temperature mismatch of 10°F , the inlet temperature error increased with increasing secondary airflow and was 1.7°F at a secondary airflow level of 13 percent of total airflow. Inlet temperature error with a mismatch of 15°F increased from 1.1 to 3.1°F as secondary airflow was increased from 5 to 13 percent of total airflow and to 3.3°F as secondary airflow was further increased to 19 percent of the total airflow.

4.2 COMPRESSION SYSTEM COMPONENTS TOTAL-PRESSURE AND TEMPERATURE PROFILES

The steady-state, total-pressure pattern produced by the AJDG was in good agreement ($RMSE \leq 2.5$ percent) with that produced by the inlet screens. The differences in total-pressure profiles at the engine were attenuated by the compression system components as shown in Fig. 17. For the hub radial distortion pattern, engine inlet profile differences of three percent were reduced such that there was no measurable difference in the total-pressure profiles at the inlet to the high-pressure compressor (surge component).

The total-temperature profiles at the compression system component measuring stations are presented in Fig. 18. The uniform engine inlet temperature with distortion produced by the screen and AJDG system is reflected in the total-temperature profiles through the compressors. At each measuring station, the total-temperature profiles with screen and AJDG distortion agree within 0.5 percent.

4.3 ENGINE STABILITY RESPONSE

The currently accepted method of producing steady-state, total-pressure distortion for turbine engine stability testing uses the technique of installing various porosity screens in the engine inlet. In order for the AJDG to be an acceptable alternate method, it is necessary to define any differences in engine stability with distortion produced by the two methods. During this test, engine stability was determined for three parametric distortion patterns produced by inlet screens and by the AJDG system. The test procedure provided a direct comparison of engine operation with the same steady-state distortion pattern produced by the two methods. Engine stability was also determined with and without the airjet struts installed (no secondary airflow) to evaluate the effects of the struts on the clean inlet flow pattern.

4.3.1 AJDG Installed, No Secondary Airflow

In order to increase the test configuration flexibility, it is desirable to have the capability of conducting either clean inlet or distortion testing with the same hardware installation. Baseline engine stability was determined without the airjet struts installed and with the airjet struts installed but with no secondary airflow.

The steady-state, inlet distortion level was not affected by the installation of the AJDG struts. For both installations, the inlet distortion (P2DIST) was nominally 0.5 percent at the highest corrected airflow (WA2R2 = 200 lbm/sec). Inlet total-pressure turbulence was less than one percent for both installations.

Engine bypass ratio and rotor speed ratio is presented as a function of engine pressure ratio in Fig. 19. Bypass ratio followed the expected trend of decreasing with increasing engine pressure ratio. Rotor speed ratio increase during engine loading corresponded to the increase in engine power level required to maintain a constant engine airflow.

The operating maps for the three compression system components (fan, intermediate compressor, and high-pressure compressor) are presented in Fig. 20. The operating path of each component was controlled by the loading technique used during the surge testing. The fan pressure ratio was increased by reducing the engine exhaust nozzle area, and total airflow was maintained constant by increasing the engine power setting. The HPC pressure ratio was increased by in-bleeding air to the HPC discharge. The increase in engine power setting required to maintain constant engine airflow resulted in an increase in HPC airflow. The intermediate pressure compressor moved along its normal operating line as the engine power was increased.

The high-pressure compressor normal operating line (operation with no inbleed and at design nozzle area) was not affected by the installation of the airjet struts (Fig. 20). With the engine loaded according to the previously described procedure, HPC surge occurred with no engine inlet distortion. There was no discernible difference in the HPC surge lines for the two undistorted (clean) inlet configurations. The HPC surge margin was approximately 20 percent over the range of HPC corrected airflow from 46 to 51 lbm/sec.

The normal operating line for the fan was the same for both undistorted (clean) inlet configurations (Fig. 20). Variations in the fan pressure ratio with the different HPC surges are the result of the nonrepeatability of the engine loading.

The normal operating line for the intermediate pressure compressor (IPC) was unchanged for the two undistorted (clean) inlet configurations (Fig. 20). The operating point of the

IPC at the time of the HPC surge was dependent on the engine power level.

4.3.2 Parametric Inlet Distortion Patterns

The engine stability response to three basic parametric inlet distortion patterns (180 deg, tip radial, and hub radial) was determined. Each pattern was first produced with an inlet screen and then the screen pattern was reproduced with the AJDG system. Engine stability testing was accomplished with the three basic patterns at nominal engine airflow rates (WA2R2) of 170 and 200 lbm/sec. Engine loading was accomplished in the manner previously described for the undistorted (clean) inlet surge testing.

180-deg Distortion Pattern

A high-pressure compressor surge occurred with the 180-deg inlet distortion pattern and the fan and high-pressure compressor loading. The operating map for the high-pressure compressor with the 180-deg engine inlet distortion pattern imposed is presented in Fig. 21.

The HPC normal operating levels with the 180-deg AJDG pattern were within one percent of the normal operating line with screen distortion. The HPC surge point repeatability with distortion produced by each method (screen and AJDG) was approximately two percent. The average HPC surge pressure ratio with the AJDG produced 180-deg distortion patterns, one percent lower than the surge line defined with screen-produced distortion.

Tip Radial Distortion Pattern

A fan surge occurred with the tip radial pattern imposed at the engine inlet and the engine loaded as described in Section 3.3. The operating map for the fan with tip radial engine inlet distortion is presented in Fig. 22.

At the lower engine airflow (WA2R2 \approx 170 lbm/sec), the fan normal operating level with AJDG-produced tip radial distortion was approximately one percent lower than the normal operating level with screen-produced distortion. There was no discernible difference in the fan normal operating levels with distortion produced by the two methods (screen and AJDG) at the higher engine airflow (WA2R2 \approx 200 lbm/sec). At the lower engine airflow (WA2R2 \approx 170 lbm/sec), the fan surge pressure ratios with AJDG distortion ranged from one to three percent lower than the fan surge

line with inlet screen distortion. At the higher engine airflow (WA2R2 \approx 200 lbm/sec), the fan surge pressure ratios with AJDG distortion agree with the surge line defined with screen distortion within one percent.

Hub Radial Distortion Pattern

The combination of the hub radial engine inlet distortion pattern and the engine loading resulted in an HPC surge. The high-pressure compressor operating map with hub radial engine inlet distortion is presented in Fig. 23.

The high-pressure compressor normal operating line was essentially the same with distortion produced by the two methods (screen and AJDG) with deviations less than one percent. The HPC surge pressure ratios were lower with AJDG-produced distortion than the surge line defined with screen distortion. At the lower engine airflow (WA2R2 \approx 170 lbm/sec), the HPC surge with AJDG distortion occurred at pressure ratios ranging from four to seven percent below the surge line defined with screen distortion. High-pressure compressor surge pressure ratios at the higher engine airflow (WA2R2 \approx 200 lbm/sec) were seven to eleven percent lower than the surge line with screen distortion.

4.4 EVALUATION OF DIFFERENCES BETWEEN SCREENS AND THE AJDG AS DISTORTION SYSTEMS

Significant differences were determined between the engine surge margin with screen and AJDG distortion. These differences are probably the result of differences in the dynamic flow field at the engine inlet. The instrumentation used for this test was not sufficient for a quantitative assessment of the time variant inlet flow-field characteristics; however, a qualitative assessment can be made of the dynamic characteristics. In this discussion, a simplified model of the dynamic flow field is presented along with its relation to the engine surge margin.

4.4.1 Inlet Flow-Field Dynamic Characteristics

The difference in inlet turbulence measured with screen and AJDG distortion is indicative of a difference in flow-field dynamic characteristics downstream of the distortion generating devices. The flow field downstream of the AJDG may be associated with three flow zones (1) uniform mixing zone - that area downstream of the counterflowing jets that is affected only by the pressure loss mechanism of counterflow, (2) nonmixing zone - that area downstream of the

nonflowing jets that is unaffected by the flowing jets, and (3) nonuniform mixing zone - that area that encompasses the transition from the uniform mixing zone to the nonmixing zone. The relative extent of each flow zone for a specified distortion level (P2DIST) is dependent on the pattern characteristics (shape and proximity of low-pressure boundary to duct wall), primary air velocity, and secondary airflow rate. The progressive increase in the size of the nonuniform mixing zone that occurs with increasing secondary airflow and decreasing primary air velocity is shown schematically for a hub radial pattern in Fig. 24. The nonuniform mixing zone can range from a small part of the area (Fig. 24a) to the extreme condition at which the nonuniform mixing zone becomes large enough to completely eliminate the nonmixing zone (Fig. 24c).

The size of the nonuniform mixing zone is reflected by the extent of total-pressure loss across the inlet duct in the area of nonflowing airjets. For the hub radial pattern produced by the AJDG system, a total-pressure loss extended across the entire radius of the inlet duct (Fig. 25). The flow field associated with the AJDG hub radial pattern then conformed to the dynamic flow field in which nonuniform mixing occurs over the majority of the flow area, and an area of nonmixing does not exist.

For this inlet flow field, it is surmised that the highest turbulence levels occur in the nonuniform mixing zone. The AJDG system then produced a hub radial pattern that included a relatively large area with the highest turbulence. This is dissimilar to that obtained with the distortion screen. As shown in Fig. 25, the extent of the high shear zone associated with the screen was small, relative to that for the AJDG as reflected by the absence of total-pressure loss in the undistorted (clean) area.

4.4.2 Accountability of Inlet Pattern Differences for Loss of Engine Surge Margin

As described earlier, the steady-state inlet patterns produced by the two methods (screen and AJDG) were in good agreement. Steady-state, total-pressure and total-temperature profiles at the various compression system component measuring stations were essentially the same for both distortion methods. The measured turbulence was higher and occurred in a larger area with the AJDG pattern than with the screen distortion pattern.

The compressor stability margin is affected by both the turbulence level and the amount of flow area associated with each turbulence level. The qualitative results of this test indicate that the AJDG patterns differed from the screen patterns in both of these areas. It is surmised that these differences are responsible for the measured difference in engine surge margin with inlet distortion produced by the two methods.

5.0 SUMMARY OF RESULTS

A performance evaluation of the AJDG system was conducted for three parametric and one composite total-pressure distortion patterns. Engine stability margin was determined and compared for inlet total-pressure distortion produced by inlet screens and the AJDG system. Significant results of this evaluation are summarized as follows:

1. The root mean square error of the steady-state, inlet total-pressure pattern produced by the AJDG system ranged from 1.0 to 2.3 percent for the parametric patterns. This error is less than that normally obtained for screens using current design techniques.
2. The repeatability of the AJDG-produced, constant, composite, total-pressure distortion pattern was 0.4 percent over a range of corrected engine airflow from 160 to 240 lbm/sec.
3. The AJDG system produced a specified inlet distortion pattern within two minutes after command. The pattern set time demonstrates the increased flexibility of the AJDG as compared with a normal screen development time of approximately 12 working days.
4. Local inlet turbulence levels, ($\Delta PRMS/P_2$), measured with screen distortion were less than one percent. Local turbulence levels measured with AJDG distortion were highest (six percent) for the hub radial pattern and lowest (two percent) for the 180-deg pattern.

5. The AJDG supply air-conditioning system maintained the secondary air temperature within $\pm 3^{\circ}\text{F}$ of the primary air total temperature. At the temperature match level of $\pm 3^{\circ}\text{F}$, there is no discernible engine inlet total-temperature error.
6. Installation of the airjet struts in the inlet ducting, without airjet airflow, did not affect the clean inlet pattern. There were no measurable differences in engine surge margin with a clean inlet with and without the airjet struts installed. Clean inlet high-pressure compressor surge margin was 20 percent over the range of corrected high-pressure compressor airflow from 46 to 51 lbm/sec.
7. The high-pressure compressor surge pressure ratios with the 180-deg distortion pattern were approximately one percent lower with AJDG distortion than with screen distortion.
8. A fan surge occurred with the tip radial distortion pattern imposed at the engine inlet with both screens and AJDG. At the higher engine airflow (200 lbm/sec), there was no difference in the fan pressure ratio at surge with the two methods of producing inlet distortion. At the lower engine airflow (170 lbm/sec), the fan pressure ratio at surge was approximately two percent lower with AJDG distortion than with screen distortion.
9. High-pressure compressor surge occurred at pressure ratios ranging from four to eleven percent lower with AJDG hub radial distortion than for the screen-produced pattern.
10. Qualitative analysis of test results indicates the area of high shear turbulent mixing that separates the relatively uniform flow areas of high and low total pressure at the engine inlet is larger with AJDG distortion than with screen distortion.
11. It is surmised that the larger areas of high turbulence associated with the AJDG distortion pattern was the cause of the differences in engine surge margin.

REFERENCES

1. Parker, J. R., Lazalier, G. R., and Rakowski, W. J. "Effects of Time Variant Inlet Distortion on Compressor Stability Characteristics of an Augmented Turbofan Engine at Reynolds Number Indices 0.6, 0.3, and 0.15." AEDC-TR-71-150 (AD886069L), July 1971.
2. Stevenson, C. W. and Rakowski, W. J. "Evaluation of an Airjet System for Producing Steady-State Total Pressure Distortion at the Inlet of Turbine Engines." AEDC-TR-73-68 (AD910303L), May 1973.
3. Test Facilities Handbook (Tenth Edition). "Engine Test Facility, Vol. 2." Arnold Engineering Development Center, May 1974.
4. Owens, C. L. "Calibration Capabilities of the ESF Instrument Branch." AEDC-TR-67-18 (AD648707), March 1967.
5. National Aeronautics and Space Administration, U. S. Standard Atmosphere, 1962.
6. Military Specification, MIL-E-5008C, Engine, Aircraft, Turbojet and Turbofan, Model Specification for December 30, 1965.
7. Abernethy, Dr. R. B., et al., Pratt and Whitney Aircraft, and Thompson, J. W., Jr., ARO, Inc. "Handbook Uncertainty in Gas Turbine Measurements." AEDC-TR-73-5 (AD755356) February 1973.
8. Smith, Robert E., Jr. and Matz, Roy J. "Verification of a Theoretical Method of Determining Discharge Coefficients for Venturis Operating at Critical Flow Conditions." AEDC-TR-61-8 (AD263714), September 1961.
9. Wolff, H. E. "Calibration of Three Venturi Airflow Metering Systems with Sting-Mounted Centerbodies at Critical and Subcritical Flow Conditions." AEDC-TR-66-52 (AD632085), May 1966.

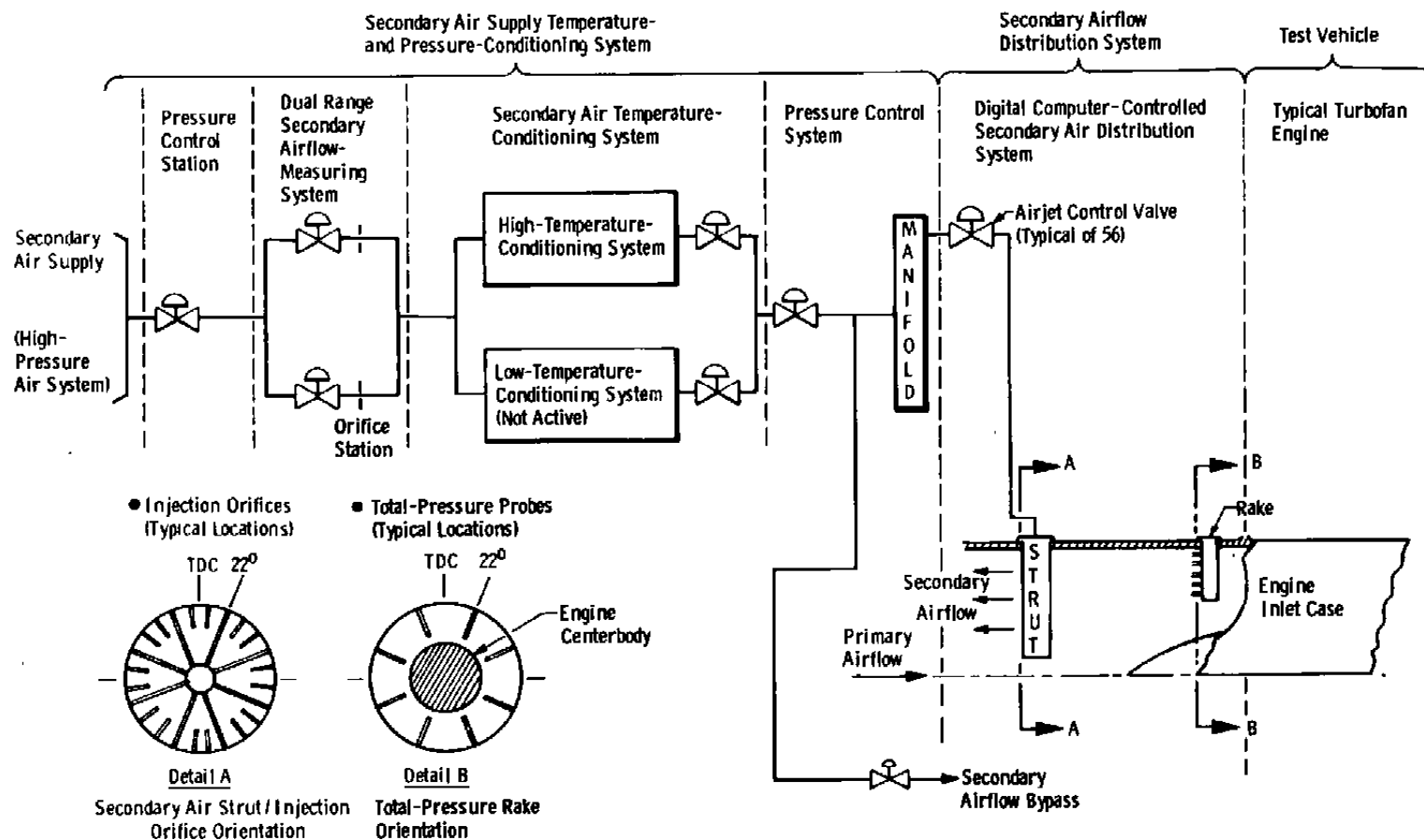
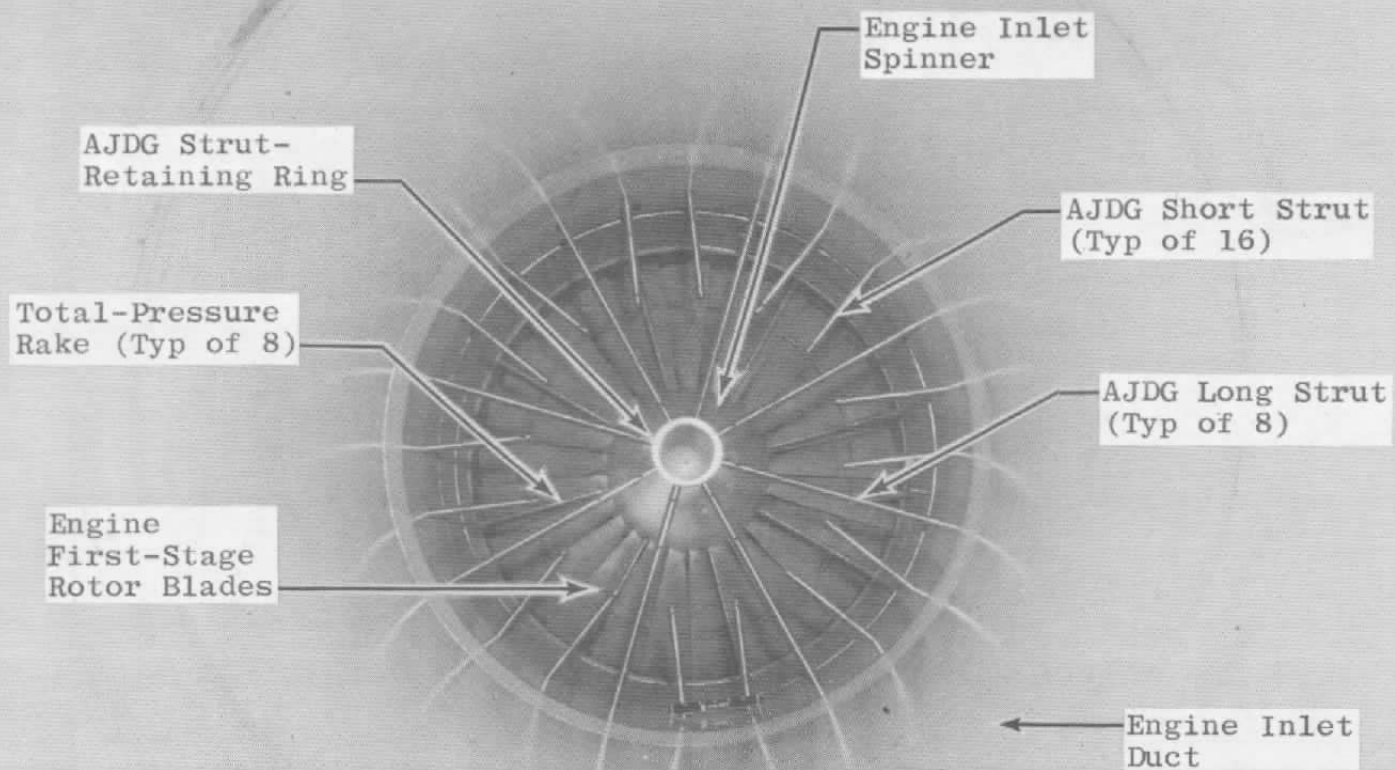
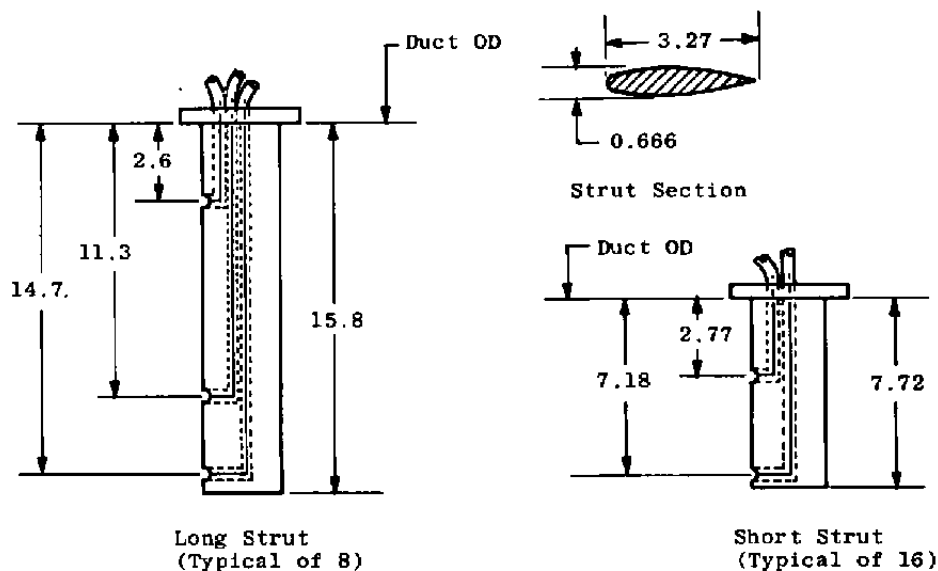


Figure 1. Functional schematic of the airjet distortion generator system.



A E D C
10019-75

a. Installation in engine air supply duct
Figure 2. Airjet distortion generator strut details.

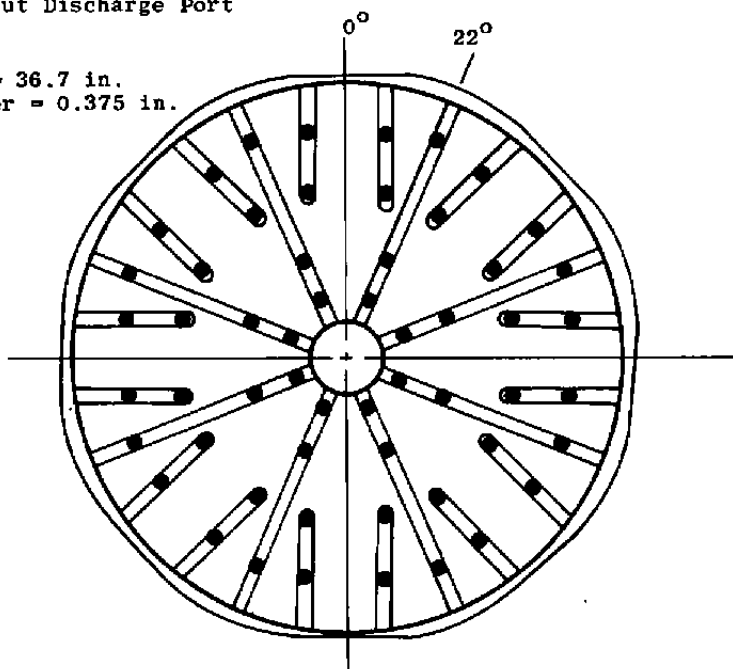


Strut Details

All Dimensions in Inches

● Strut Discharge Port

Duct Diameter = 36.7 in.
Orifice Diameter = 0.375 in.



Secondary Air Strut/Injection
Orifice Orientation
(View Looking Downstream)

b. Dimensional schematic
Figure 2. Concluded.

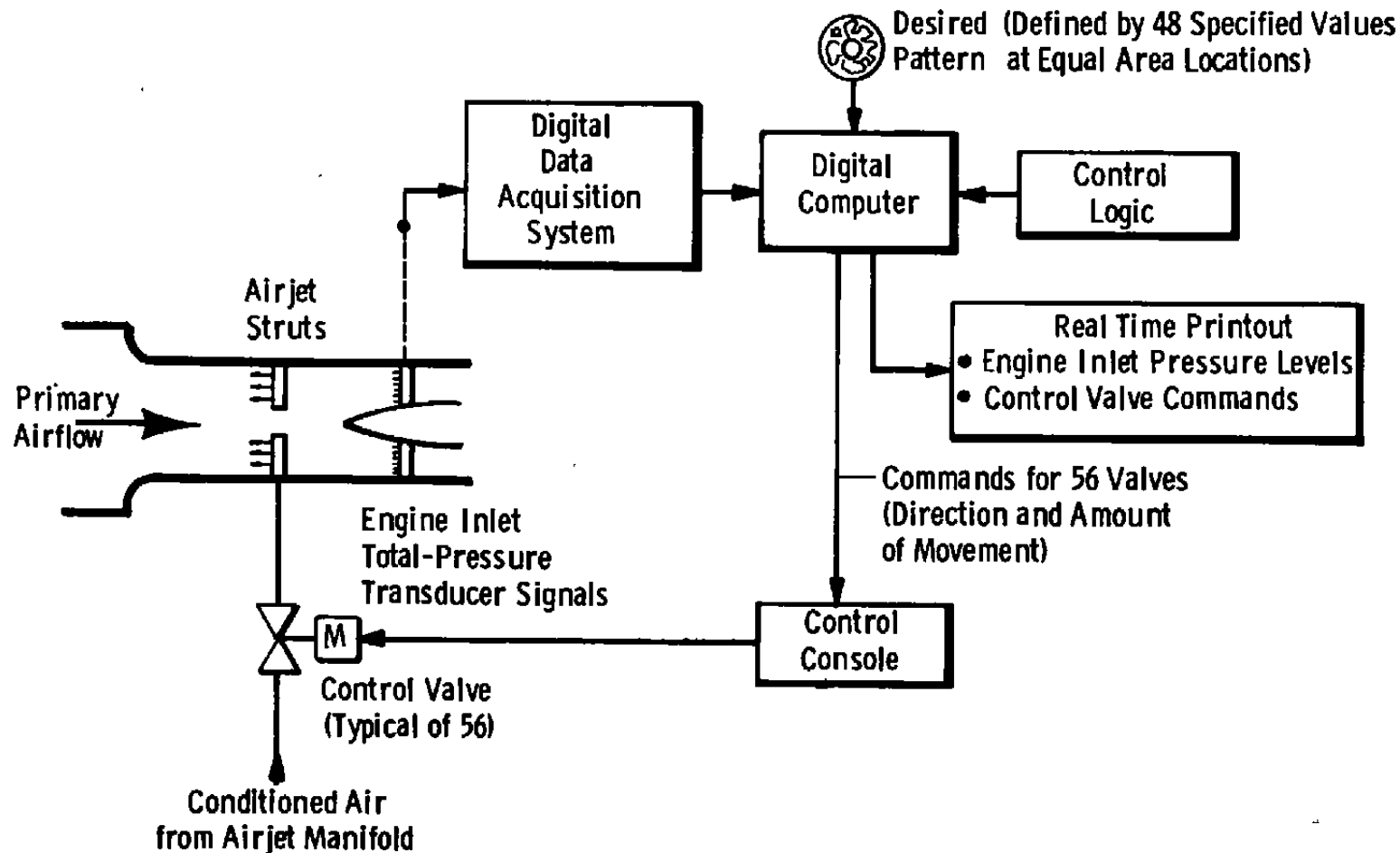


Figure 3. Functional schematic of the airjet distortion generator airflow distribution control system.

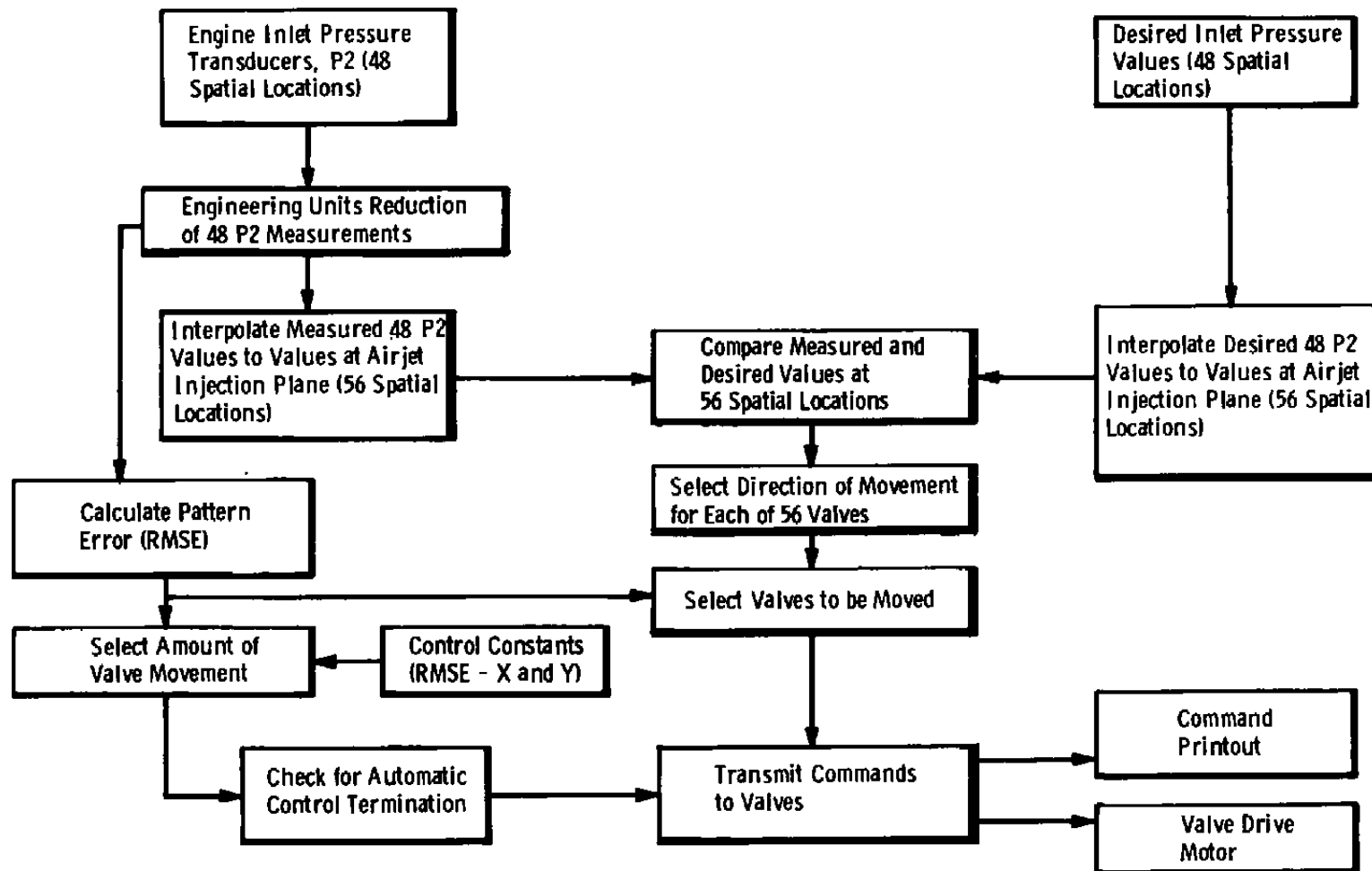


Figure 4. Computer control logic for airjet distortion generator airflow distribution system.

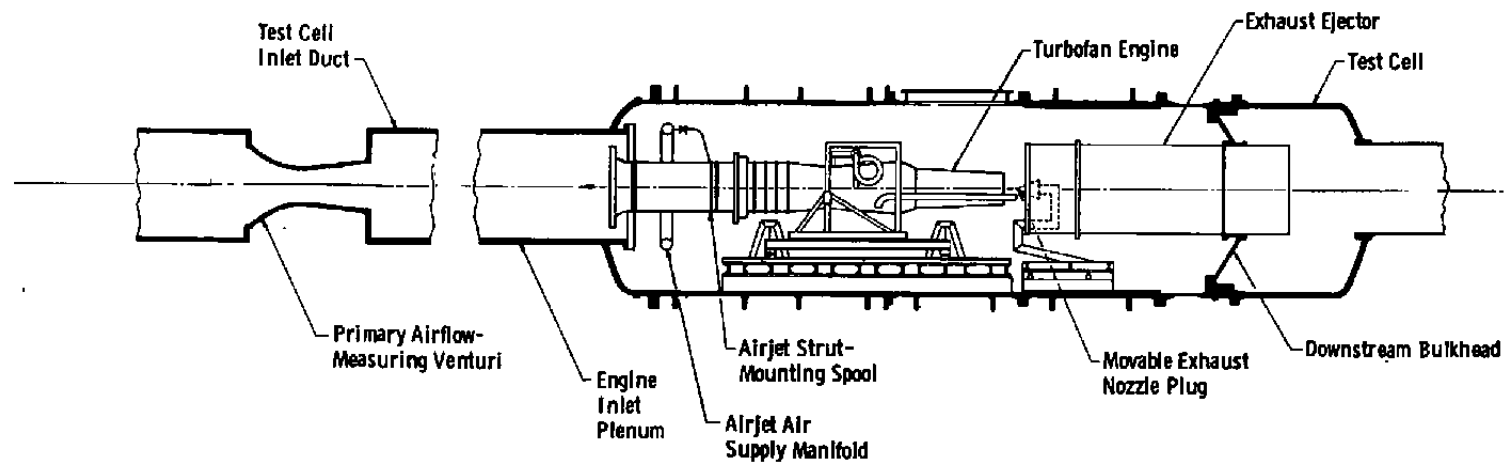
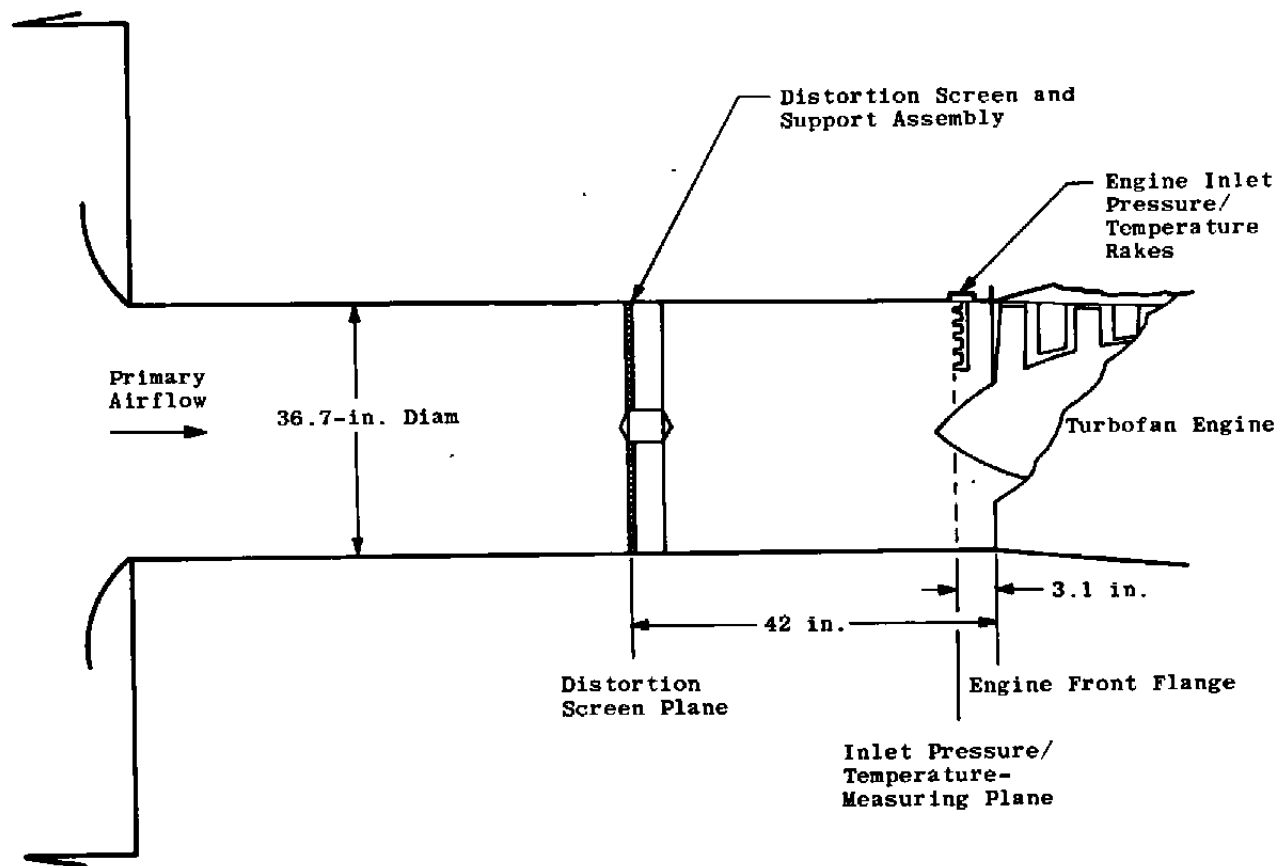
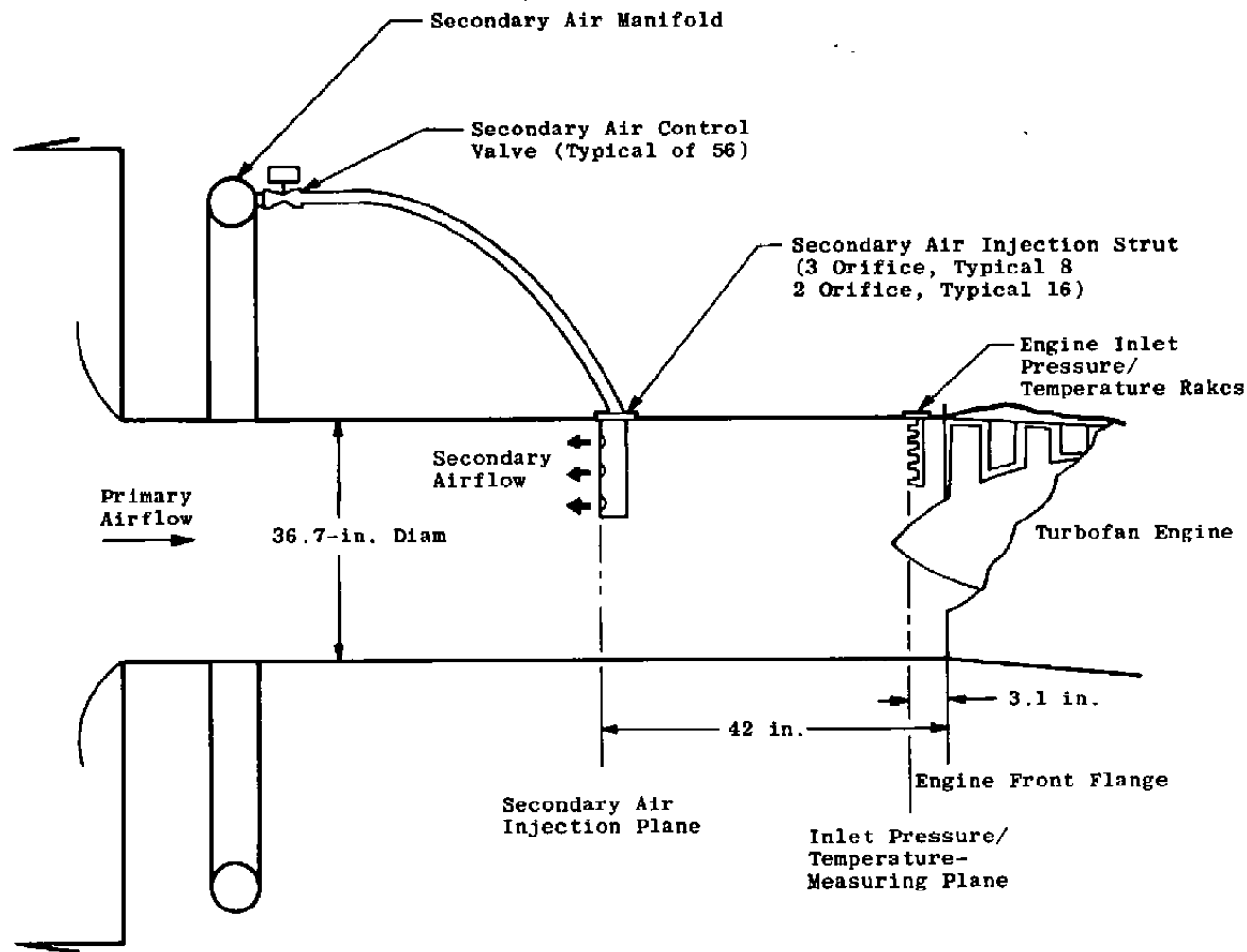


Figure 5. Airjet distortion generator/engine installation in altitude test cell.



a. Distortion screen installed
 Figure 6. Engine inlet duct configuration details.



b. Airjet distortion generator struts installed
Figure 6. Concluded.

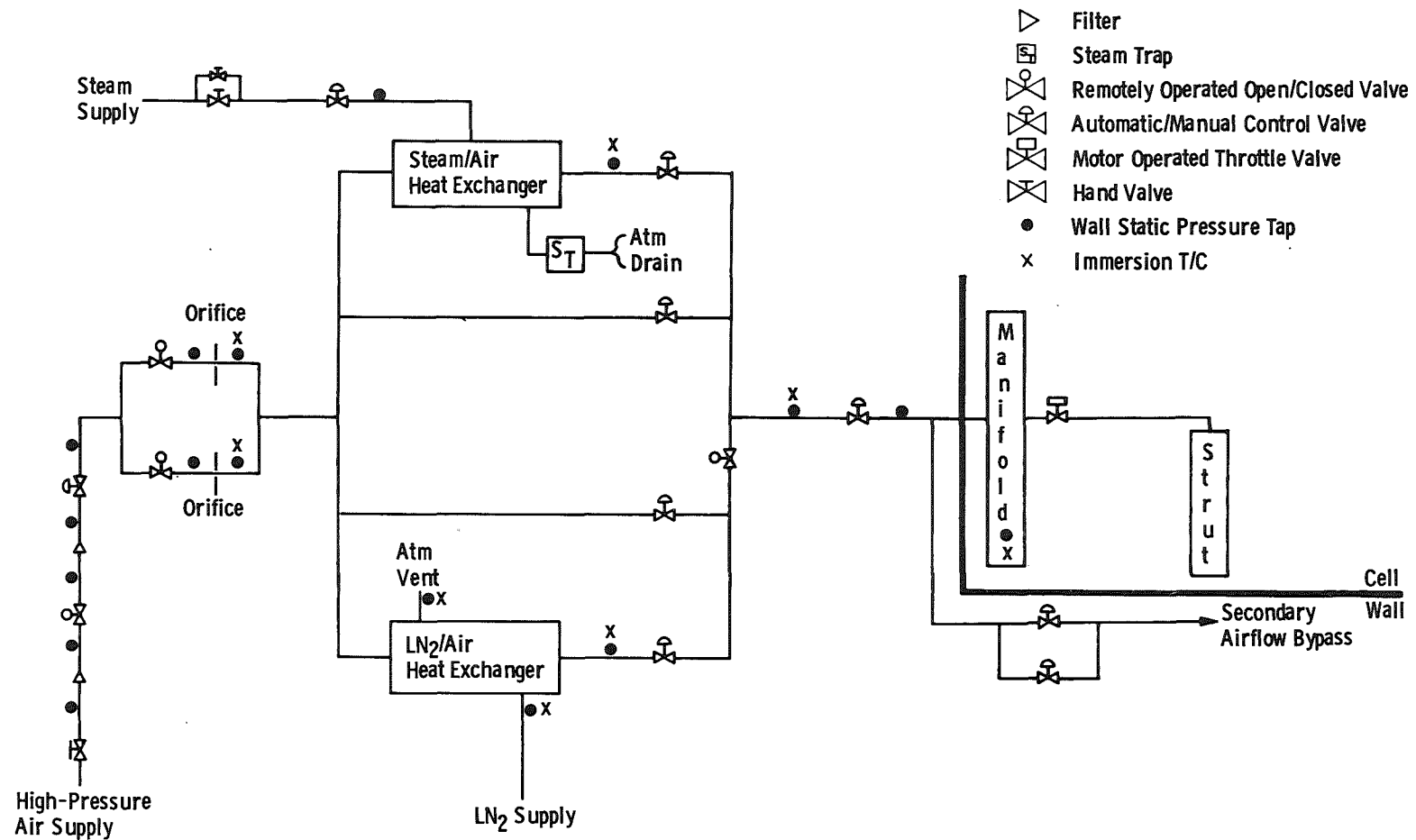
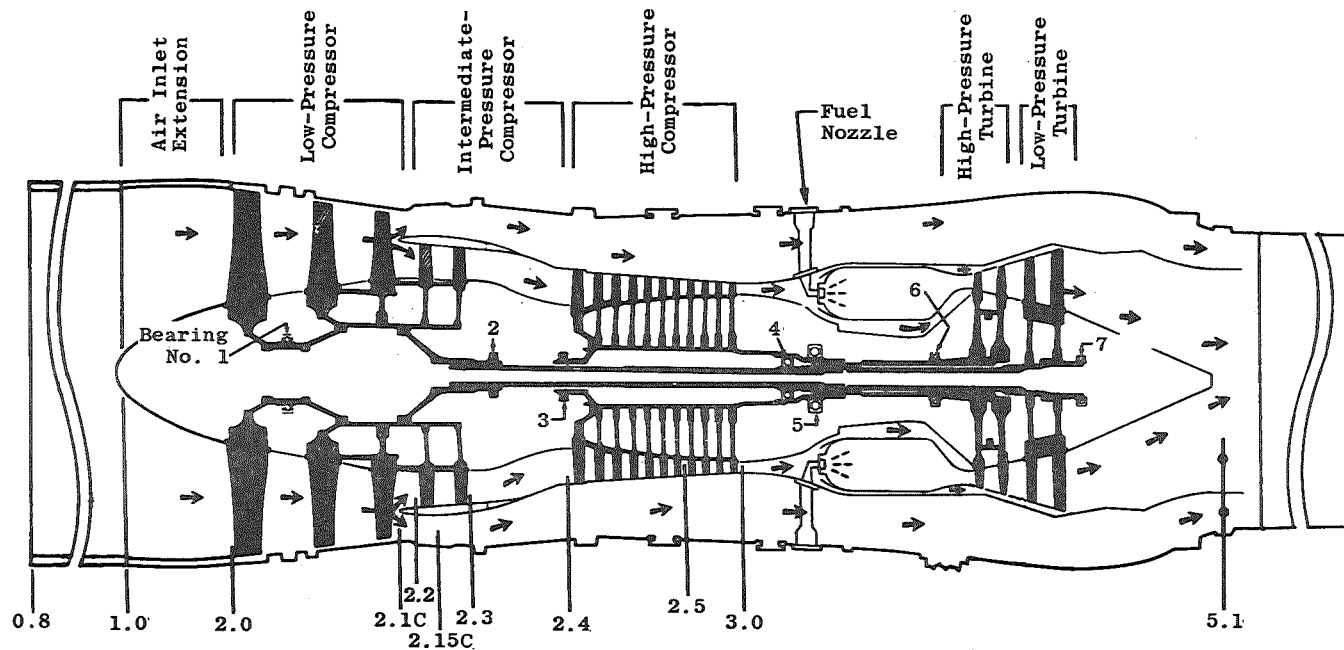


Figure 7. Airjet distortion generator air supply system instrument locations.



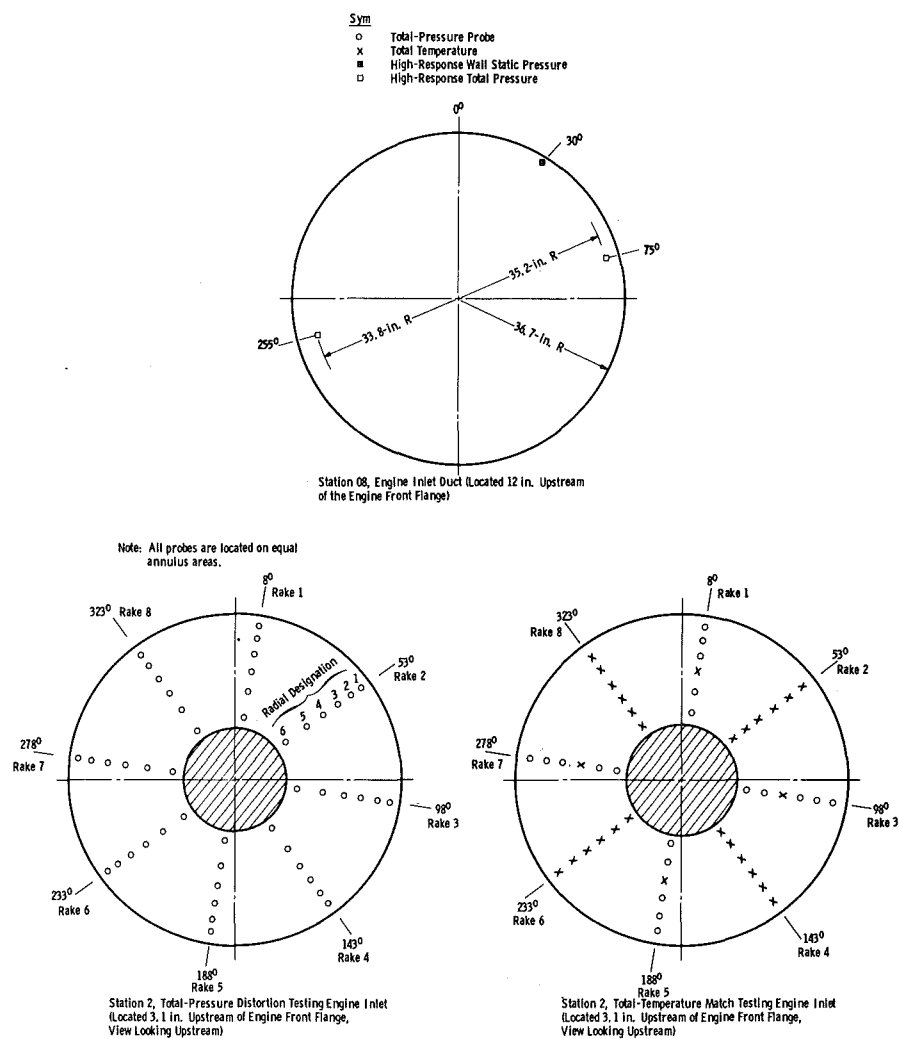
Station	0.8	2	2.1C	2.2	2.15C	2.3	3	5.1
Total Pressure		48 ¹	5	5	5	3	5	18 ²
High-Response Total Pressure	2							
Total Temperature		28 ³		5	5	3	5	8
High-Response Wall Static Pressure			1			1	1	
Close Coupled Wall Static Pressure							1	

¹Reduced to 20 for Temperature Match Test

²Manifolded

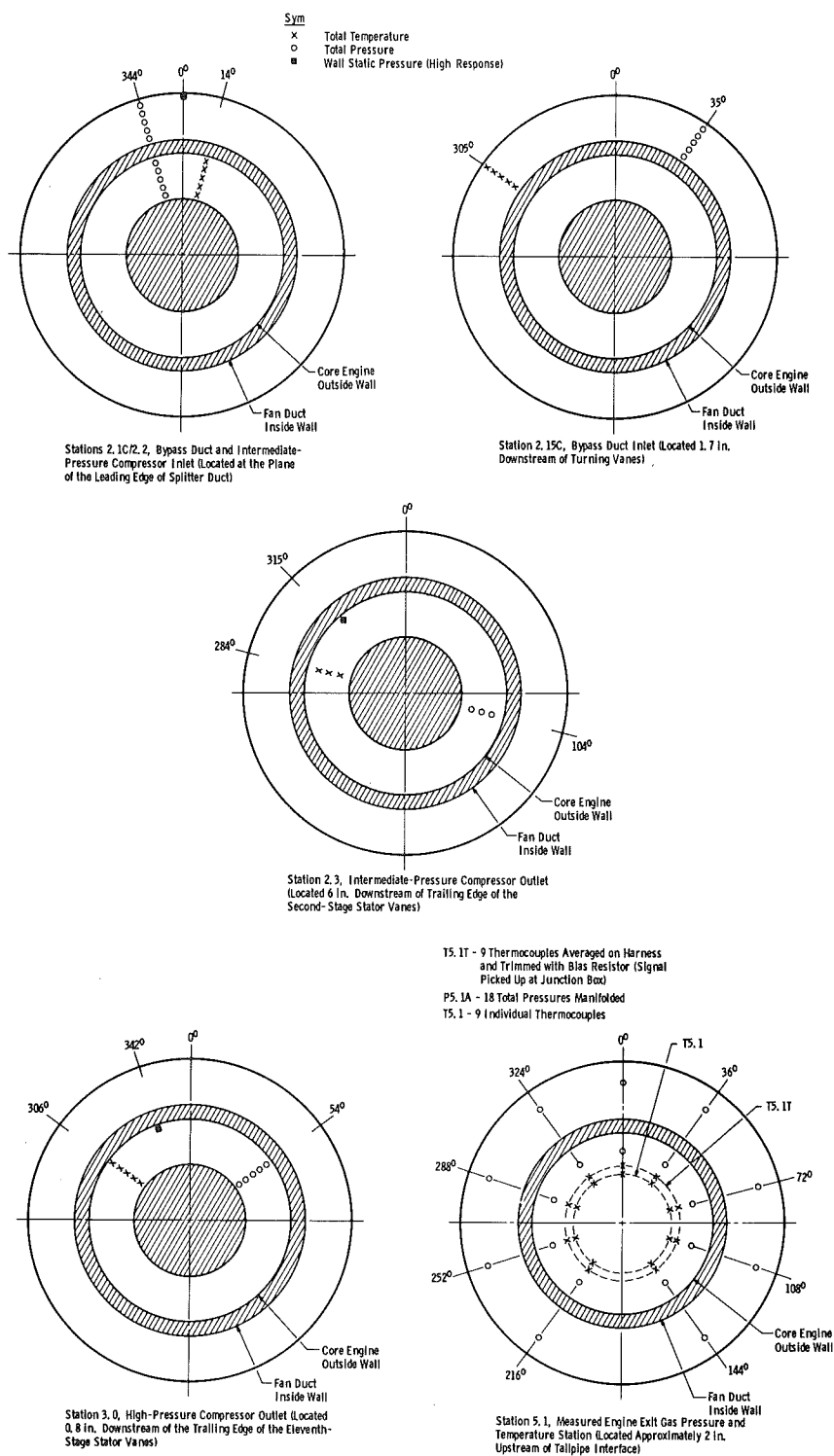
³Installed Only for Temperature Match Test

Figure 8. Engine instrument station locations.

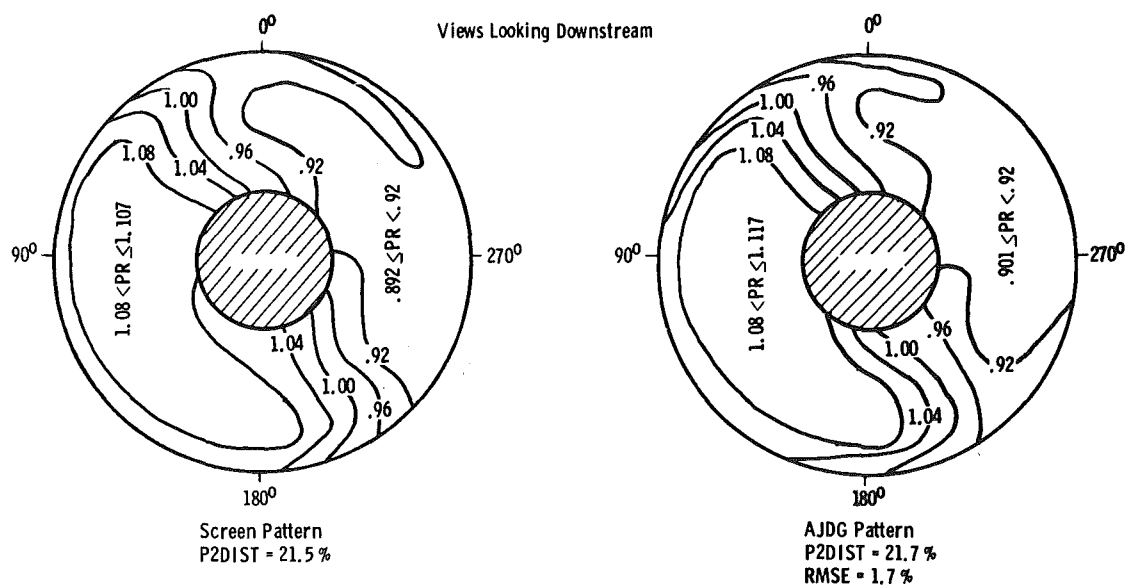


a. Engine inlet duct

Figure 9. Instrumentation details, looking upstream.



b. Engine
Figure 9. Concluded.



$$P2DIST = \frac{P2MAX - P2MIN}{P2AVG} \times 100, \text{ percent}$$

$$PRI = \frac{P2I}{P2AVG}$$

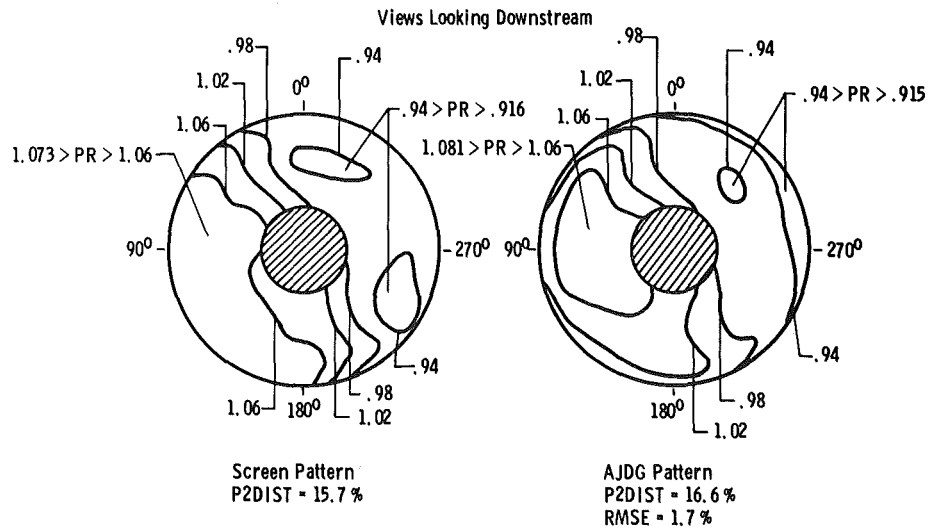
$$RMSE = \sqrt{\frac{\sum_{i=1}^N \left(\frac{PRI_{AJDG}}{PRI_{SCREEN}} - 1 \right)^2}{N}} \times 100, \text{ percent}$$

Individual Pressure Ratios (PRI) at Each of 48 Equal Area Spatial Locations

Annulus	Rake Location, deg															
	8		53		98		143		188		233		278		323	
	Screen	AJDG	Screen	AJDG	Screen	AJDG	Screen	AJDG	Screen	AJDG	Screen	AJDG	Screen	AJDG	Screen	AJDG
1	0.911	0.918	1.041	1.023	1.057	1.073	1.054	1.017	1.021	1.003	0.892	0.932	0.911	0.897	0.913	0.901
2	0.921	0.926	1.101	1.085	1.102	1.109	1.100	1.077	1.097	1.066	0.907	0.929	0.918	0.912	0.923	0.920
3	0.910	0.917	1.096	1.103	1.099	1.110	1.107	1.102	1.102	1.081	0.899	0.903	0.914	0.912	0.913	0.912
4	0.900	0.908	1.087	1.105	1.097	1.108	1.092	1.099	1.089	1.094	0.902	0.911	0.916	0.907	0.911	0.911
5	0.920	0.920	1.088	1.099	1.098	1.102	1.101	1.117	1.076	1.074	0.916	0.920	0.915	0.914	0.911	0.916
6	0.966	0.963	1.093	1.095	1.096	1.108	1.064	1.100	1.058	1.026	0.963	0.943	0.912	0.912	0.919	0.921

a. 180-deg pattern, WA2R2 = 200 lbm/sec

Figure 10. Engine inlet isobar maps for screen and airjet distortion.



$$P2DIST = \frac{P2MAX - P2MIN}{P2AVG} \times 100, \text{ percent}$$

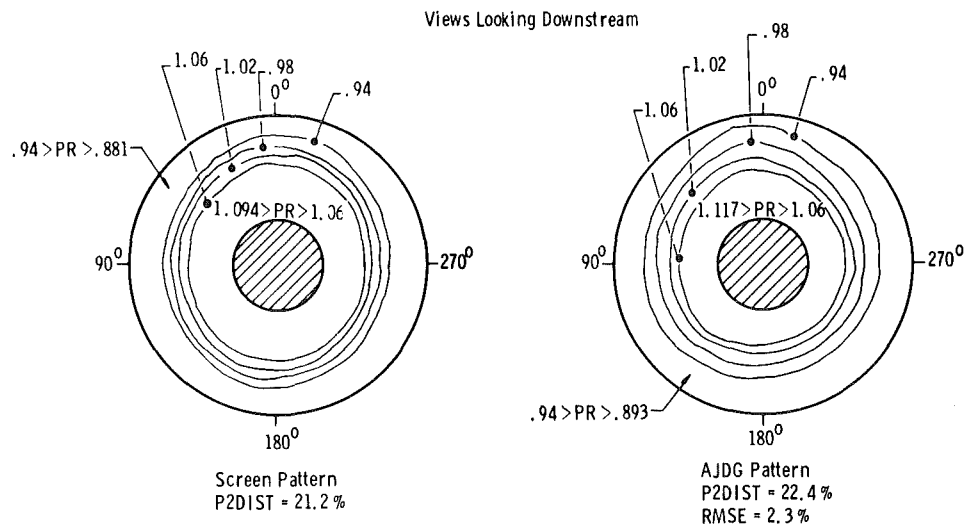
$$PRI = \frac{P2I}{P2AVG}$$

$$RMSE = \sqrt{\frac{\sum_{i=1}^N \left(\frac{PRI_{AJDG}}{PRI_{SCREEN}} - 1 \right)^2}{N}} \times 100, \text{ percent}$$

Individual Pressure Ratios (PRI) at Each of 48 Equal Area Spatial Locations

Annulus	Rake Location, deg															
	8		53		98		143		188		233		278		323	
	Screen	AJDG	Screen	AJDG	Screen	AJDG	Screen	AJDG	Screen	AJDG	Screen	AJDG	Screen	AJDG	Screen	AJDG
1	0.937	0.942	1.028	1.031	1.040	1.040	1.036	0.996	1.011	1.007	0.916	0.953	0.938	0.915	0.939	0.931
2	0.952	0.958	1.069	1.074	1.071	1.076	1.068	1.019	1.062	1.038	0.937	0.969	0.944	0.931	0.951	0.950
3	0.948	0.959	1.063	1.073	1.067	1.077	1.073	1.031	1.066	1.039	0.929	0.950	0.943	0.943	0.942	0.946
4	0.933	0.954	1.060	1.062	1.065	1.081	1.062	1.044	1.059	1.027	0.934	0.949	0.944	0.948	0.940	0.938
5	0.945	0.961	1.060	1.057	1.066	1.079	1.067	1.065	1.052	1.022	0.942	0.961	0.943	0.947	0.941	0.937
6	0.978	0.993	1.063	1.066	1.062	1.082	1.045	1.069	1.045	1.033	0.980	0.985	0.940	0.936	0.945	0.957

b. 180-deg pattern, WA2R2 = 170 lbm/sec
Figure 10. Continued.



$$P2DIST = \frac{P2MAX - P2MIN}{P2AVG} \times 100, \text{ percent}$$

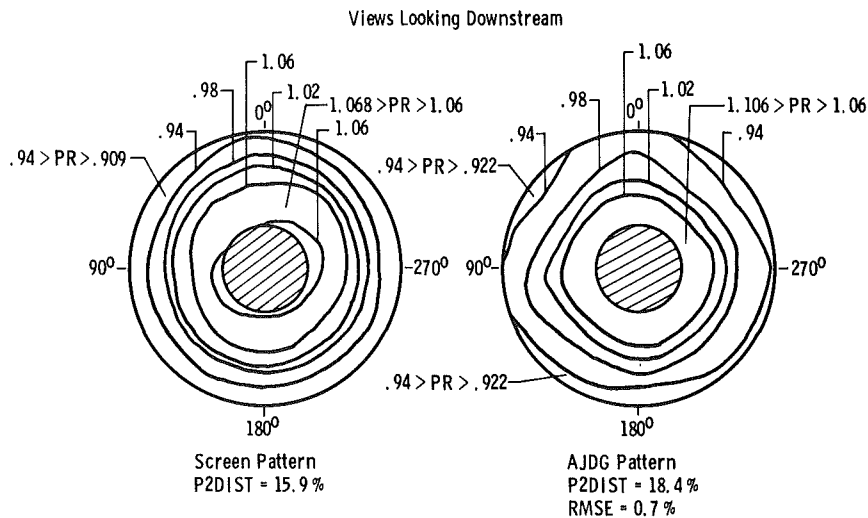
$$PRI = \frac{P2I}{P2AVG}$$

$$RMSE = \sqrt{\frac{\sum_{i=1}^N \left(\frac{PRI_{AJDG}}{PRI_{SCREEN}} - 1 \right)^2}{N}} \times 100, \text{ percent}$$

Individual Pressure Ratios (PRI) at Each of 48 Equal Area Spatial Locations

Annulus	Rake Location, deg															
	8		53		98		143		188		233		278		323	
	Screen	AJDG	Screen	AJDG	Screen	AJDG	Screen	AJDG	Screen	AJDG	Screen	AJDG	Screen	AJDG	Screen	AJDG
1	0.916	0.933	0.897	0.917	0.900	0.909	0.897	0.921	0.881	0.893	0.887	0.906	0.889	0.911	0.889	0.909
2	0.932	0.951	0.911	0.927	0.918	0.928	0.916	0.932	0.898	0.906	0.906	0.929	0.905	0.929	0.925	0.932
3	0.990	0.981	0.973	0.958	0.975	0.960	0.980	0.961	0.968	0.939	0.950	0.952	0.958	0.959	0.987	0.957
4	1.060	1.027	1.050	1.012	1.048	1.010	1.044	1.002	1.049	0.991	1.033	1.002	1.032	1.011	1.062	1.008
5	1.080	1.094	1.090	1.086	1.082	1.076	1.086	1.084	1.089	1.062	1.087	1.087	1.085	1.090	1.092	1.087
6	1.077	1.109	1.094	1.104	1.083	1.105	1.087	1.116	1.091	1.117	1.091	1.117	1.074	1.102	1.087	1.106

c. Tip radial pattern, WA2R2 = 200 lbm/sec
Figure 10. Continued.



$$P2DIST = \frac{P2MAX - P2MIN}{P2AVG} \times 100, \text{ percent}$$

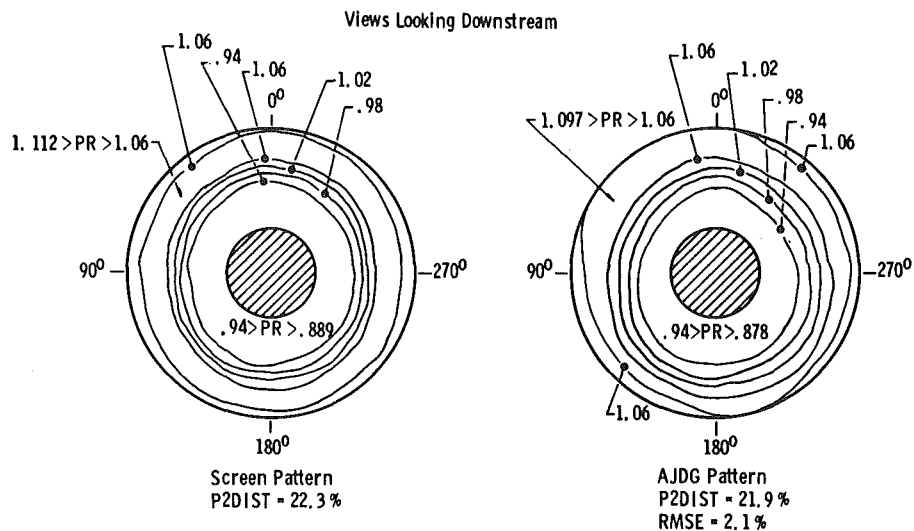
$$PRI = \frac{P2I}{P2AVG}$$

$$RMSE = \sqrt{\frac{\sum_{i=1}^N \left(\frac{PRI_{AJDG}}{PRI_{SCREEN}} - 1 \right)^2}{N}} \times 100, \text{ percent}$$

Individual Pressure Ratios (PRI) at Each of 48 Equal Area Spatial Locations

Annulus	Rake Location, deg															
	8		53		98		143		188		233		279		323	
	Screen	AJDG	Screen	AJDG	Screen	AJDG	Screen	AJDG	Screen	AJDG	Screen	AJDG	Screen	AJDG	Screen	AJDG
1	0.941	0.956	0.924	0.934	0.931	0.949	0.931	0.933	0.919	0.922	0.914	0.938	0.909	0.936	0.917	0.927
2	0.957	0.976	0.938	0.937	0.943	0.969	0.941	0.943	0.930	0.936	0.937	0.958	0.933	0.948	0.944	0.942
3	0.994	0.992	0.975	0.949	0.975	0.993	0.983	0.958	0.970	0.966	0.956	0.965	0.965	0.966	0.985	0.955
4	1.046	1.014	1.044	0.979	1.038	1.026	1.042	0.979	1.039	1.010	1.025	0.999	1.033	1.004	1.050	0.977
5	1.055	1.063	1.063	1.044	1.058	1.064	1.061	1.037	1.061	1.063	1.060	1.063	1.064	1.065	1.065	1.035
6	1.057	1.094	1.068	1.089	1.058	1.087	1.061	1.092	1.065	1.106	1.065	1.099	1.050	1.081	1.062	1.082

d. Tip radial pattern, WA2R2 = 170 lbm/sec
Figure 10. Continued.



$$P2DIST = \frac{P2MAX - P2MIN}{P2AVG} \times 100, \text{ percent}$$

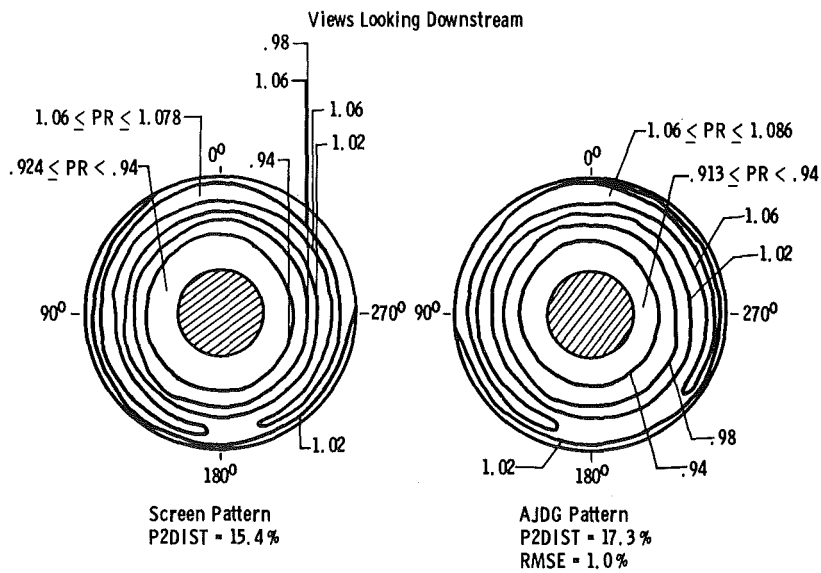
$$PRI = \frac{P2I}{P2AVG}$$

$$RMSE = \sqrt{\frac{\sum_{i=1}^N \left(\frac{PRI_{AJDG}}{PRI_{SCREEN}} - 1 \right)^2}{N}} \times 100, \text{ percent}$$

Individual Pressure Ratios (PRI) at Each of 48 Equal Area Spatial Locations

Annulus	Rake Location, deg															
	8		53		98		143		188		233		279		323	
	Screen	AJDG	Screen	AJDG	Screen	AJDG	Screen	AJDG	Screen	AJDG	Screen	AJDG	Screen	AJDG	Screen	AJDG
1	1.069	1.096	1.032	1.085	1.033	1.064	1.024	1.006	1.004	1.071	1.036	1.050	1.055	1.062	1.054	1.054
2	1.111	1.092	1.100	1.088	1.103	1.090	1.099	1.074	1.095	1.075	1.102	1.062	1.098	1.085	1.102	1.090
3	1.073	1.050	1.065	1.058	1.080	1.057	1.070	1.040	1.058	1.046	1.052	1.020	1.073	1.048	1.058	1.060
4	0.977	0.980	0.994	1.007	1.011	1.011	0.980	0.970	0.981	0.991	0.970	0.971	0.993	0.991	0.986	1.002
5	0.902	0.921	0.913	0.945	0.920	0.934	0.909	0.918	0.905	0.922	0.903	0.927	0.919	0.935	0.917	0.943
6	0.899	0.891	0.903	0.898	0.898	0.894	0.899	0.886	0.893	0.888	0.897	0.886	0.889	0.878	0.898	0.891

e. Hub radial pattern, WA2R2 = 200 lbm/sec
Figure 10. Continued.



$$P2DIST = \frac{P2MAX - P2MIN}{P2AVG} \times 100, \text{ percent}$$

$$PRI = \frac{P2I}{P2AVG}$$

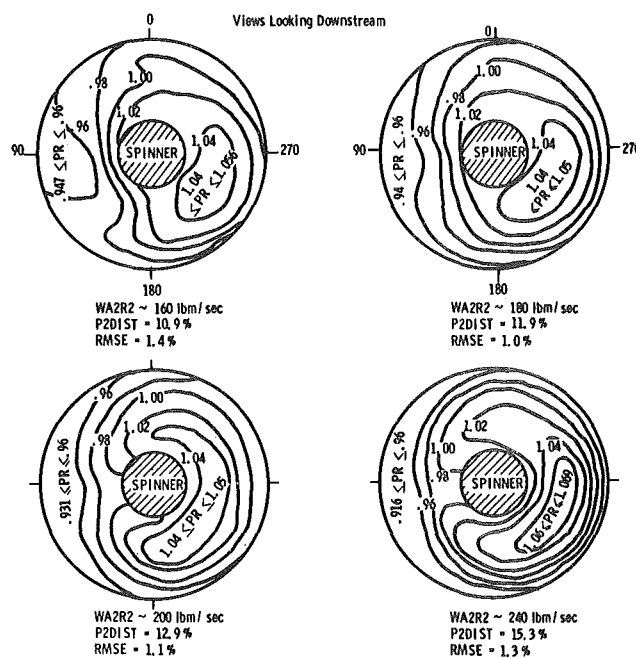
$$RMSE = \sqrt{\frac{\sum_{i=1}^N \left(\frac{PRI_{AJDG}}{PRI_{SCREEN}} - 1 \right)^2}{N}} \times 100, \text{ percent}$$

Individual Pressure Ratios (PRI) at Each of 48 Equal Area Spatial Locations

Annulus	Rake Location, deg															
	8		53		98		143		188		233		278		323	
	Screen	AJDG	Screen	AJDG	Screen	AJDG	Screen	AJDG	Screen	AJDG	Screen	AJDG	Screen	AJDG	Screen	AJDG
1	1.052	1.060	1.021	1.032	1.027	1.041	1.020	1.015	1.007	0.990	1.021	1.041	1.040	1.036	1.036	1.039
2	1.078	1.086	1.066	1.067	1.068	1.060	1.064	1.067	1.056	1.044	1.067	1.062	1.065	1.063	1.067	1.068
3	1.052	1.051	1.041	1.030	1.053	1.036	1.047	1.044	1.036	1.026	1.036	1.024	1.047	1.041	1.040	1.038
4	0.984	0.991	0.992	0.989	1.002	1.006	0.978	0.988	0.989	0.990	0.981	0.978	0.990	1.004	0.988	0.995
5	0.932	0.946	0.941	0.946	0.942	0.951	0.940	0.953	0.938	0.951	0.937	0.947	0.946	0.960	0.945	0.953
6	0.935	0.924	0.939	0.923	0.934	0.926	0.934	0.927	0.935	0.929	0.934	0.923	0.924	0.913	0.933	0.921

f. Hub radial pattern, WA2R2 = 170 lbm/sec

Figure 10. Concluded.



$$P2DIST = \frac{P2MAX - P2MIN}{P2AVG} \times 100, \text{ percent}$$

$$PRI = \frac{P2I_{AVG}}{P2AVG}$$

$$RMSE = \sqrt{\frac{\sum_{i=1}^N \left(\frac{PRI_{MEAS}}{PRI_{DES}} - 1 \right)^2}{N}}$$

Individual Pressure Ratios (PRI) at Each of 48 Equal Area Spatial Locations

	Rake Location, deg															
	8				53				98				143			
	WA2R2				WA2R2				WA2R2				WA2R2			
Annulus	160	180	200	240	160	180	200	240	160	180	200	240	160	180	200	240
1	0.989	0.981	0.973	0.964	0.963	0.954	0.943	0.930	0.947	0.940	0.931	0.916	0.974	0.952	0.943	0.918
2	0.997	0.993	0.987	0.988	0.964	0.958	0.950	0.949	0.942	0.936	0.927	0.977	0.963	0.959	0.943	
3	1.005	1.002	1.005	1.012	0.967	0.966	0.962	0.968	0.952	0.946	0.942	0.939	0.977	0.976	0.979	0.969
4	0.999	1.002	1.014	1.020	0.972	0.977	0.980	0.986	0.950	0.951	0.950	0.956	0.965	0.980	0.988	0.993
5	1.014	1.019	1.034	1.031	0.986	0.997	1.002	1.008	0.952	0.954	0.968	0.983	0.967	0.997	1.012	1.025
6	1.037	1.041	1.040	1.023	1.011	1.018	1.012	1.012	0.987	0.993	0.984	0.985	0.995	1.017	1.013	1.021

	Rake Location, deg															
	188				233				278				323			
	WA2R2				WA2R2				WA2R2				WA2R2			
Annulus	160	180	200	240	160	180	200	240	160	180	200	240	160	180	200	240
1	0.969	0.959	0.962	0.940	1.010	0.994	0.980	0.983	0.998	0.995	0.972	0.975	0.977	0.977	0.980	0.970
2	0.987	0.977	0.994	0.989	1.033	1.020	1.007	1.019	1.014	0.916	0.992	1.004	0.992	0.995	1.004	0.995
3	1.015	1.002	1.018	1.014	1.040	1.032	1.024	1.040	1.031	1.033	1.011	1.037	1.001	1.002	1.016	1.006
4	1.031	1.024	1.048	1.047	1.047	1.045	1.040	1.065	1.046	1.050	1.034	1.068	1.010	1.010	1.032	1.021
5	1.033	1.039	1.060	1.057	1.056	1.057	1.058	1.068	1.054	1.050	1.054	1.059	1.024	1.022	1.045	1.028
6	1.029	1.042	1.039	1.036	1.052	1.056	1.055	1.047	1.028	1.033	1.034	1.029	1.028	1.028	1.034	1.028

Figure 1. Engine inlet isobar maps for the airjet distortion generator-produced composite pattern.

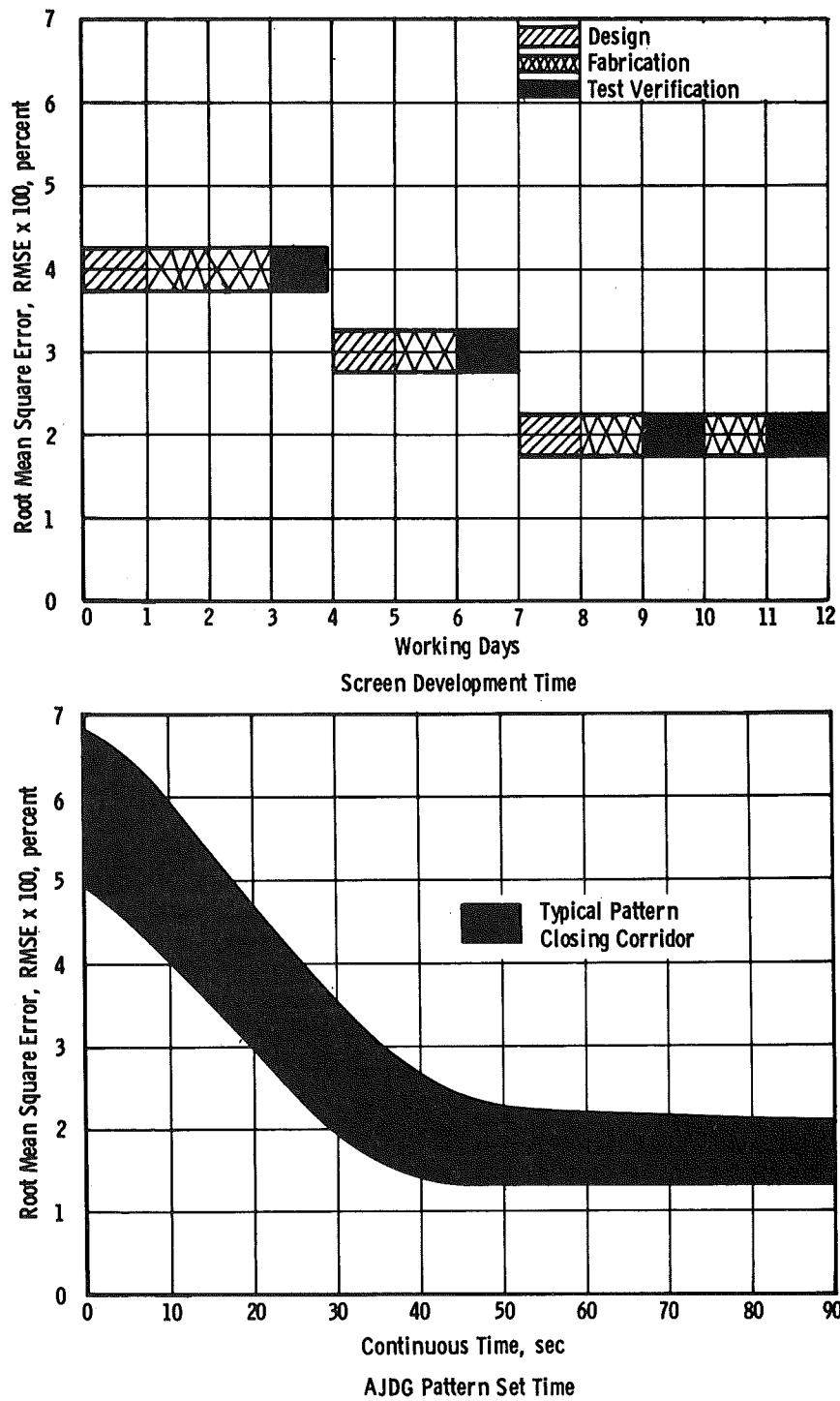


Figure 12. Relative time requirements to produce a specified distortion pattern with screens and with the airjet distortion generator system.

	WA2R2	$\Delta PRMS/P2AVG$, percent	
Distortion Screen	200	<1.0 (5 to 160 Hz)	
	170	<1.0	
Airjet System	200	2.0	
	170	2.0	

↓

Low-Pressure Area

High-Response

Total Pressure

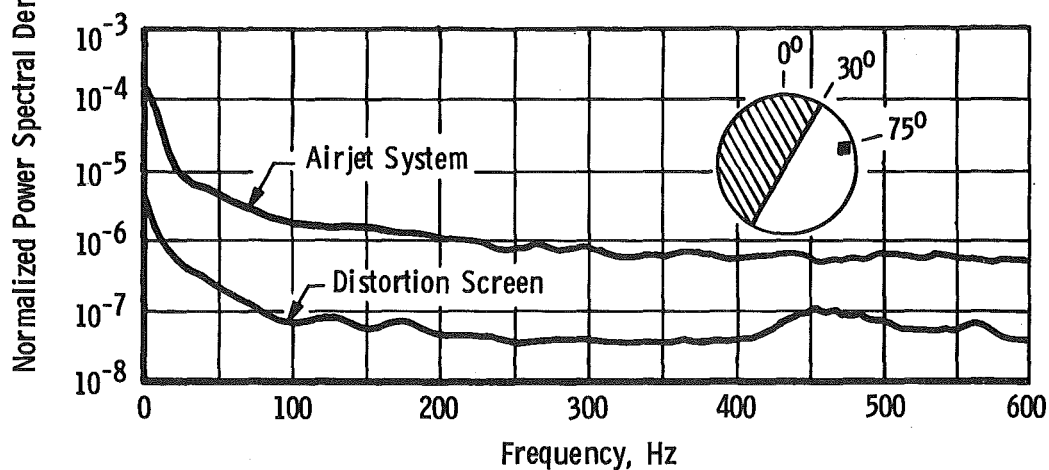
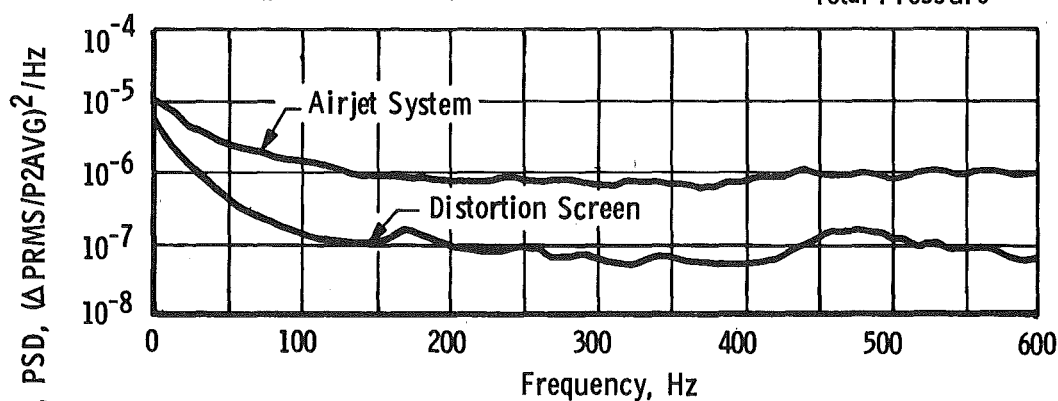
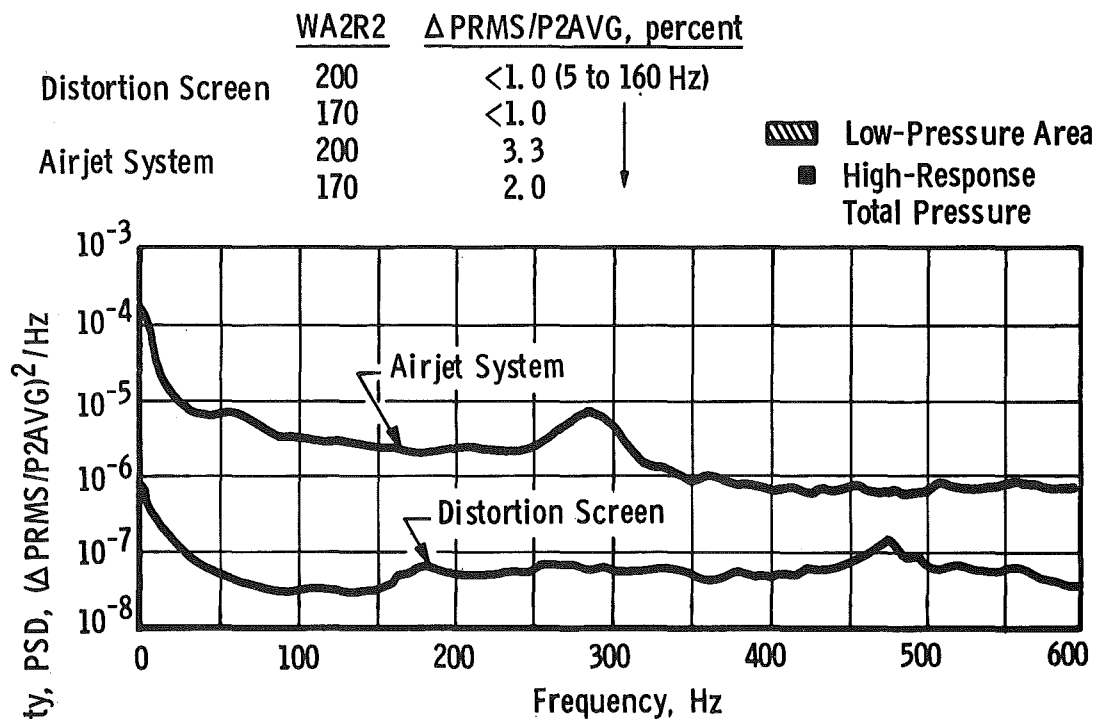
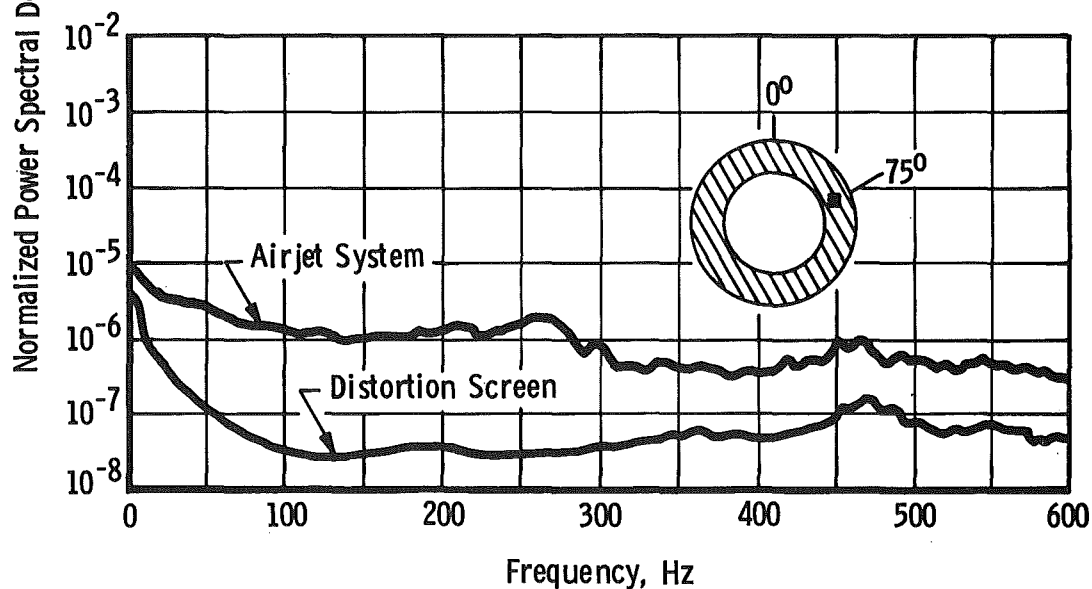


Figure 13. Power spectral density characteristics for the 180-deg distortion pattern.





a. WA2R2 = 200 lbm/sec



b. WA2R2 = 170 lbm/sec

Figure 14. Power spectral density characteristics for the tip radial distortion pattern.

	WA2R2	Δ PRMS/P2AVG, percent	
Distortion Screen	200	<1.0 (5 to 160 Hz)	
	170	<1.0	
Airjet System	200	4.9	
	170	3.9	

 Low-Pressure Area
 High-Response Total Pressure

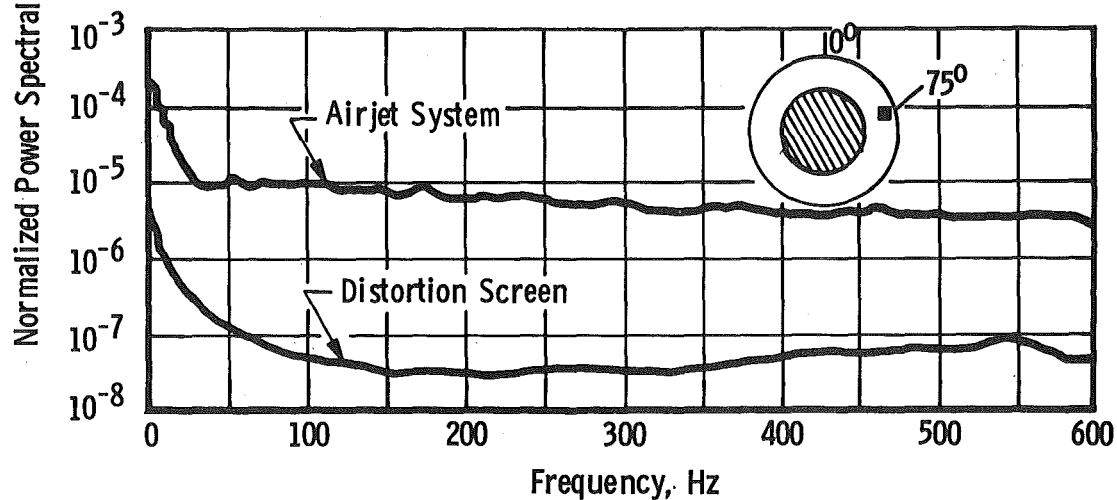
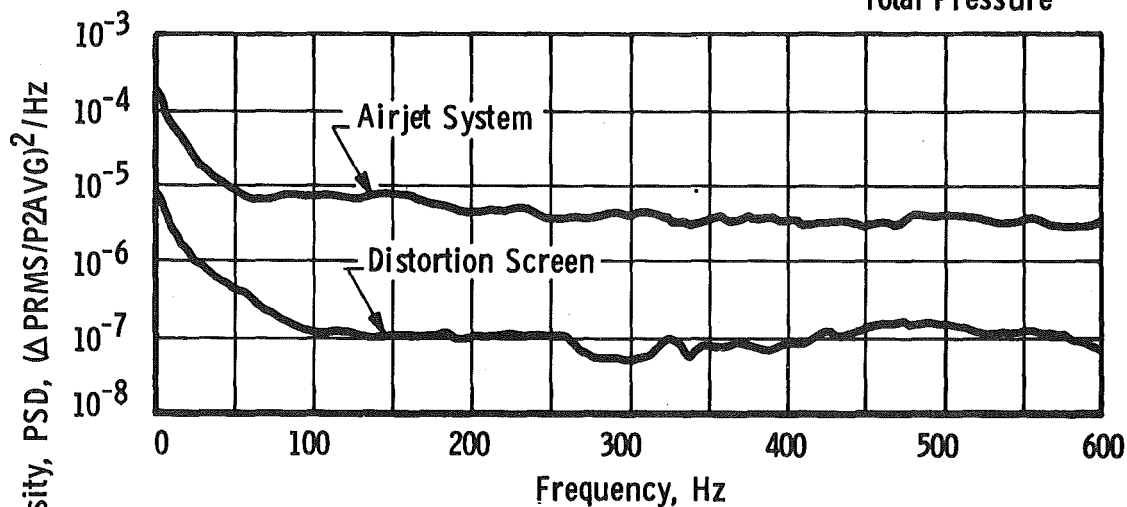


Figure 15. Power spectral density characteristics for the hub radial distortion pattern.

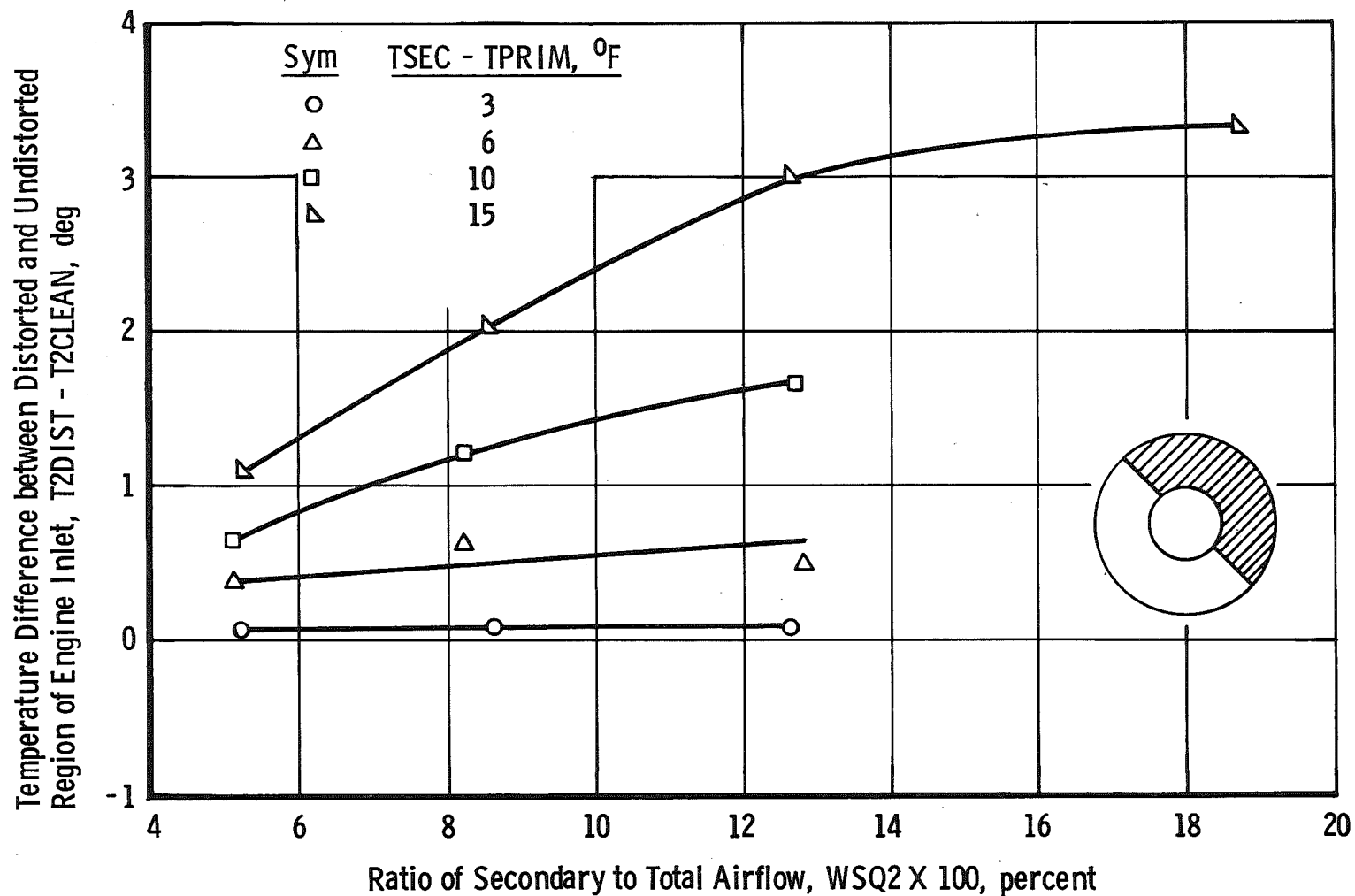


Figure 16. Effects of primary and secondary air temperature mismatch on engine inlet temperature.

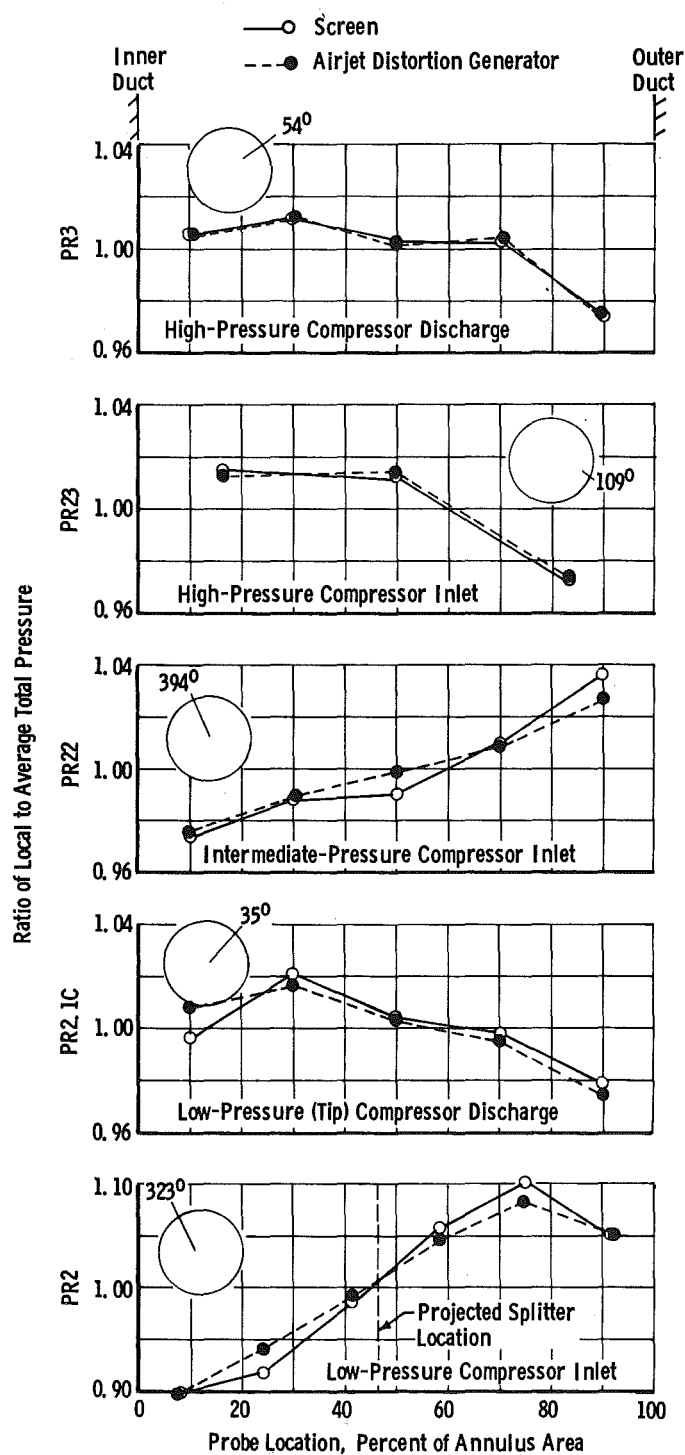


Figure 17. Comparison of compression component total-pressure profiles with screen and with airjet distortion generator hub radial distortion.

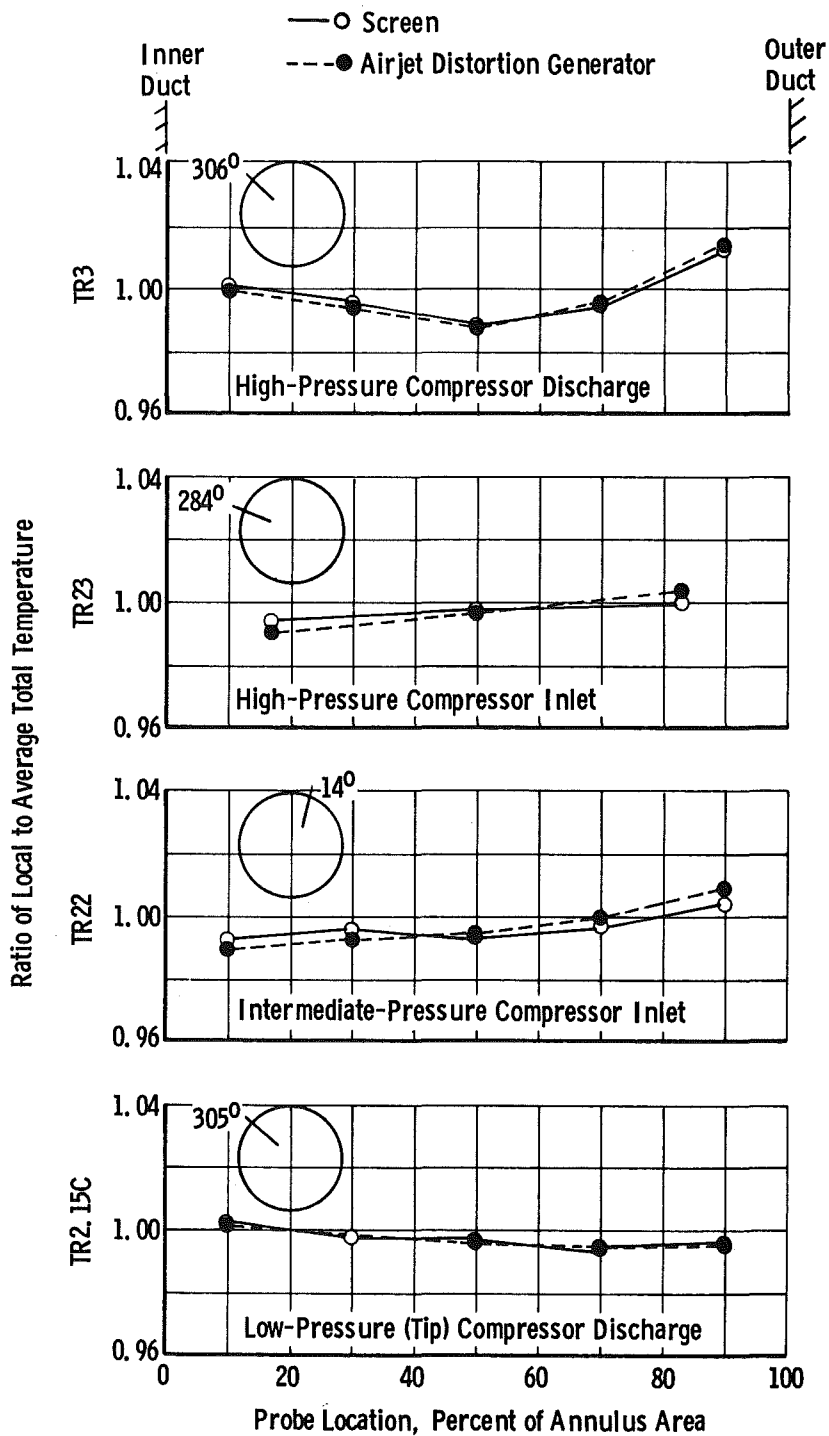


Figure 18. Comparison of compression component total-temperature profiles with screen and with airjet distortion generator hub radial distortion.

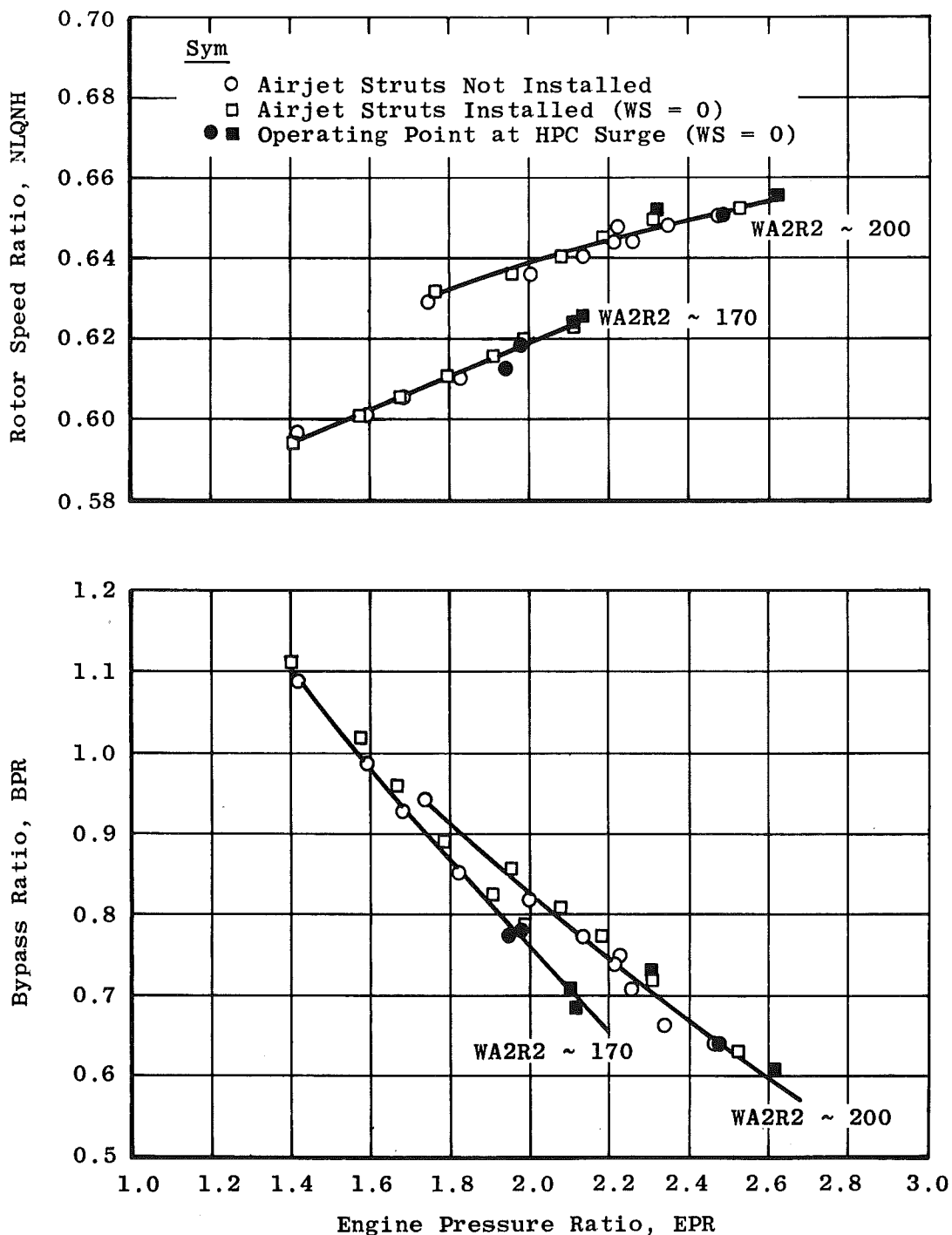


Figure 19. Effects of simultaneous loading of low- and high-pressure compressors on engine match, undistorted inlet.

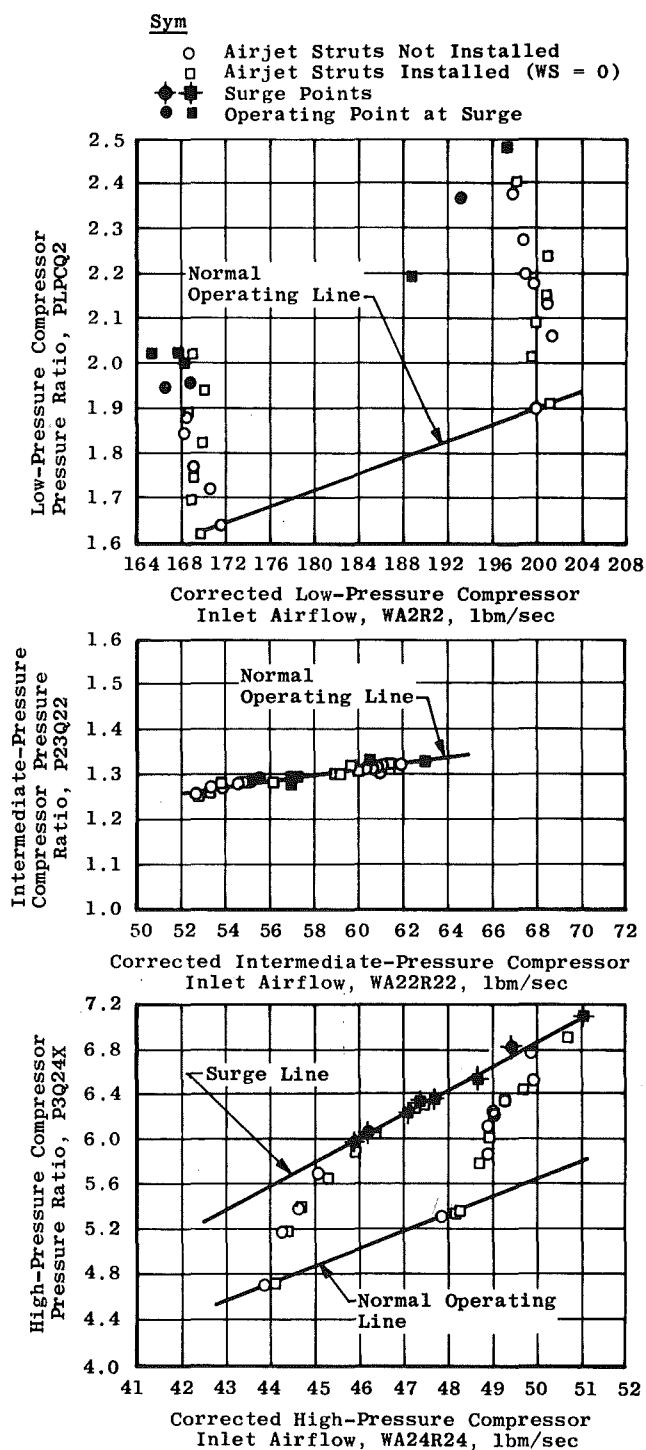


Figure 20. Compressor performance with undistorted engine inlet, 45,000 ft, Mach No. 1.2.

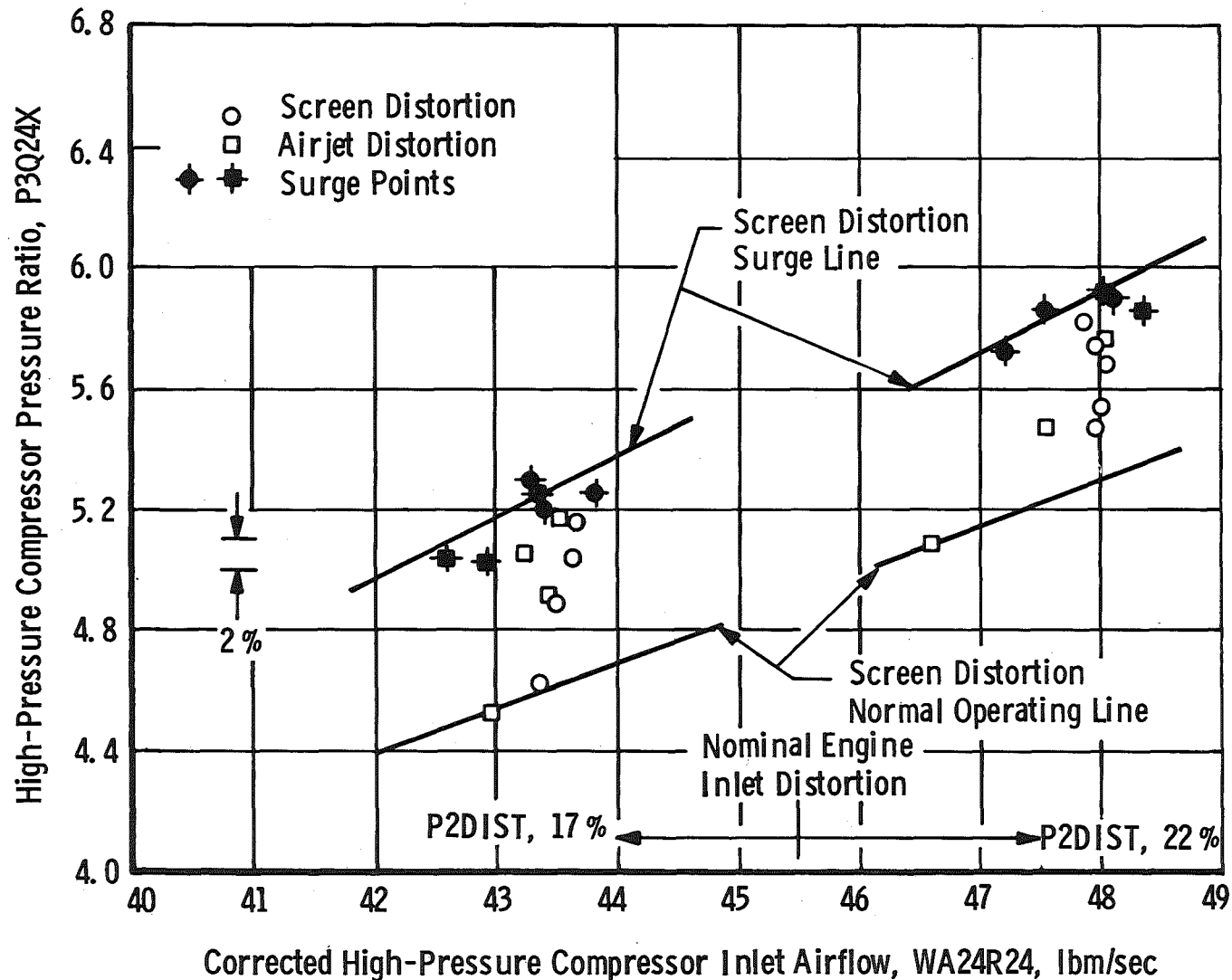


Figure 21. Comparison of high-pressure compressor performance with screen and with airjet distortion generator 180-deg engine inlet distortion pattern, 45,000 ft, Mach No. 1.2.

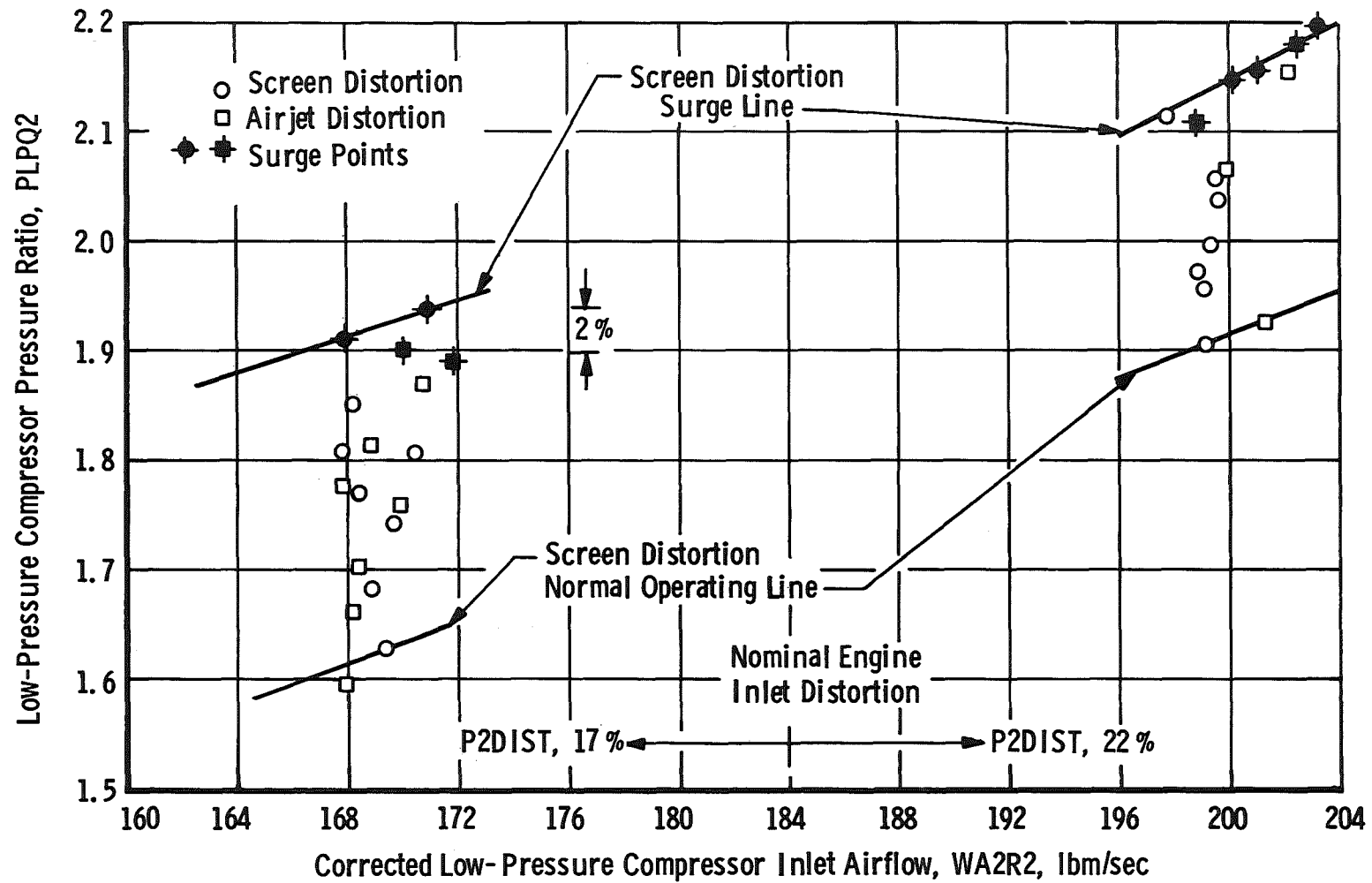


Figure 22. Comparison of low-pressure compressor performance with screen and with airjet distortion generator tip radial engine inlet distortion pattern, 45,000 ft, Mach No. 1.2.

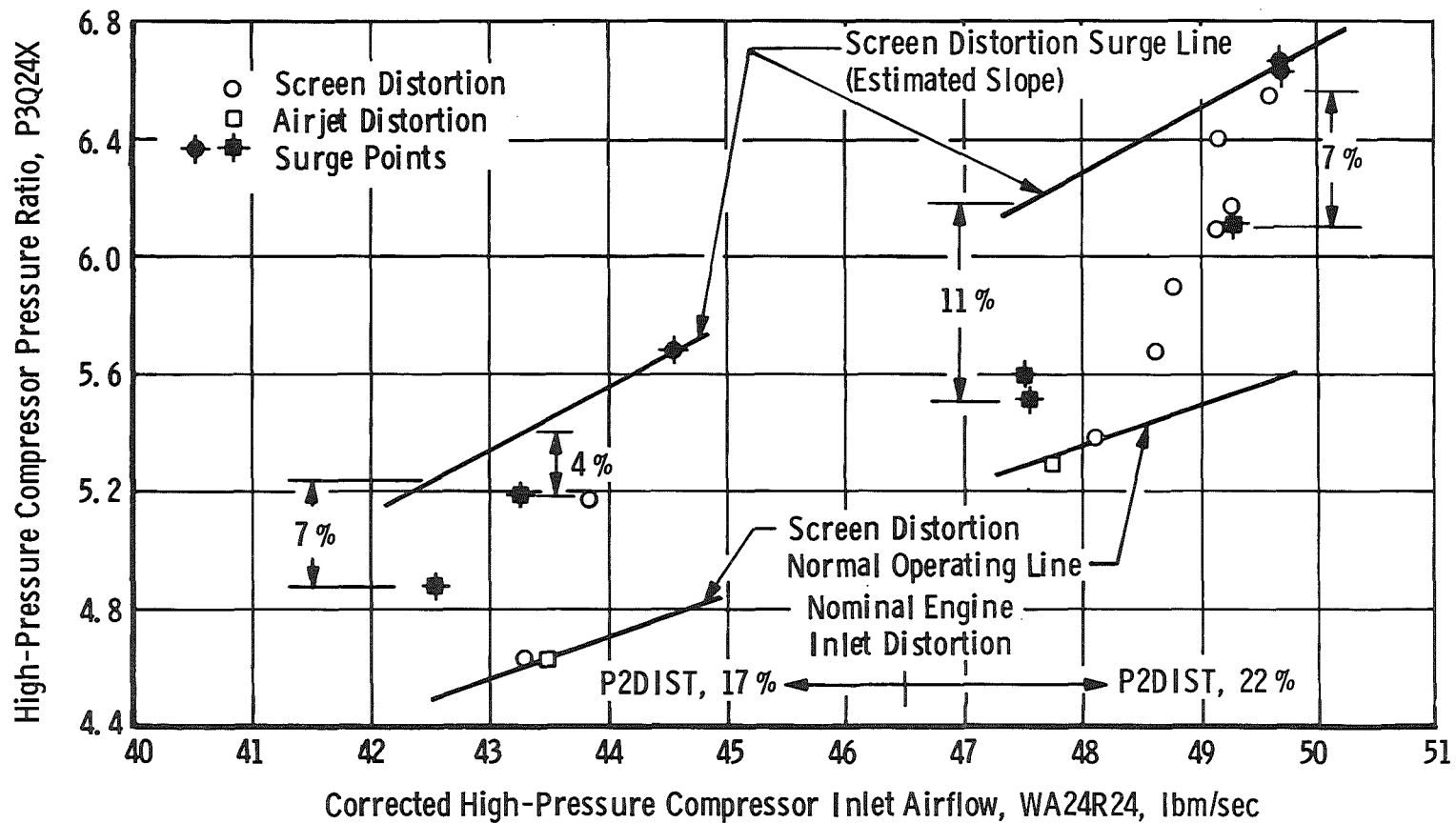


Figure 23. Comparison of high-pressure compressor performance with screen and with airjet distortion generator hub radial engine inlet distortion pattern, 45,000 ft, Mach No. 1.2.

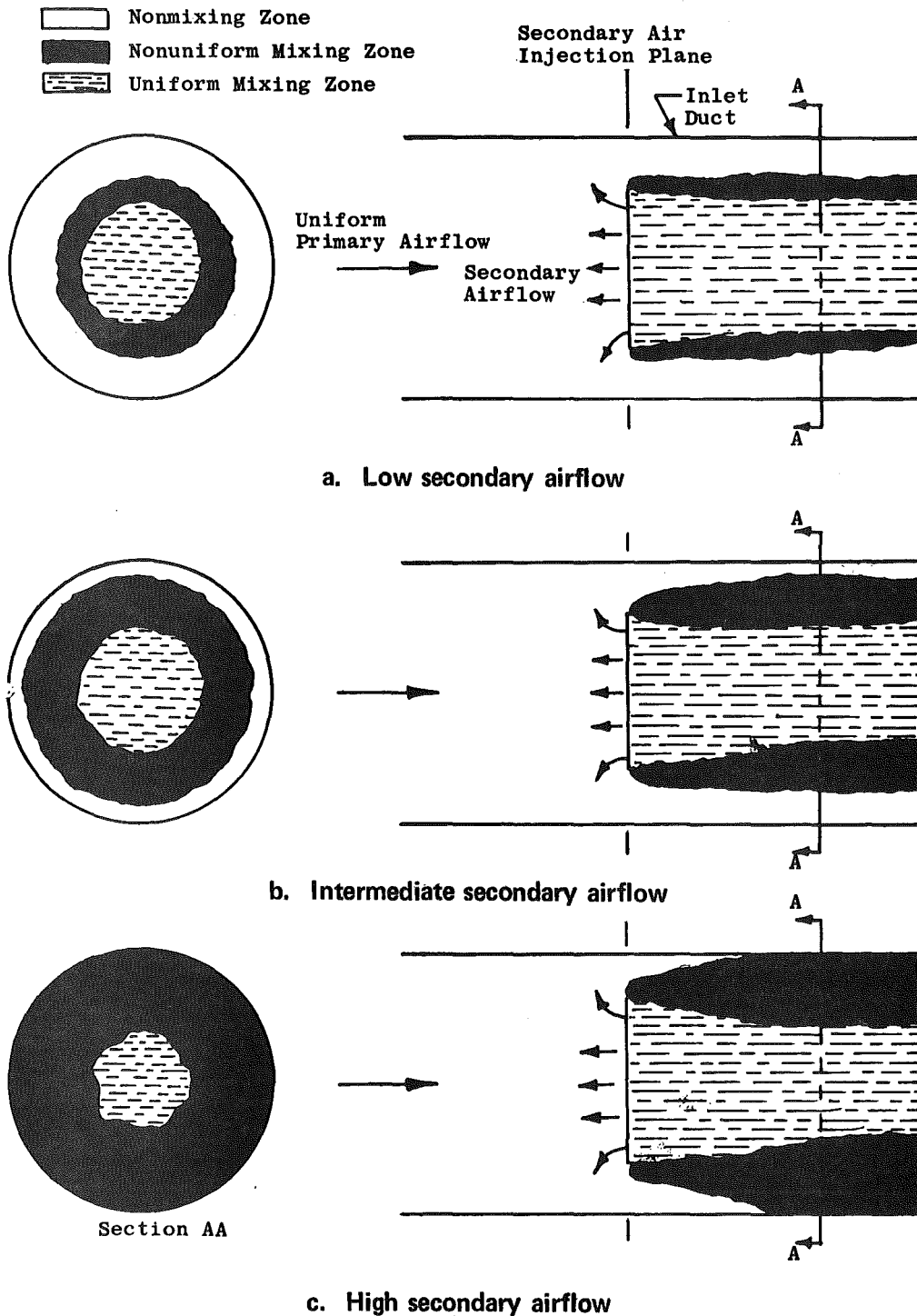


Figure 24. Schematic representation of the dynamic flow field existing with airjet distortion generator hub radial distortion patterns.

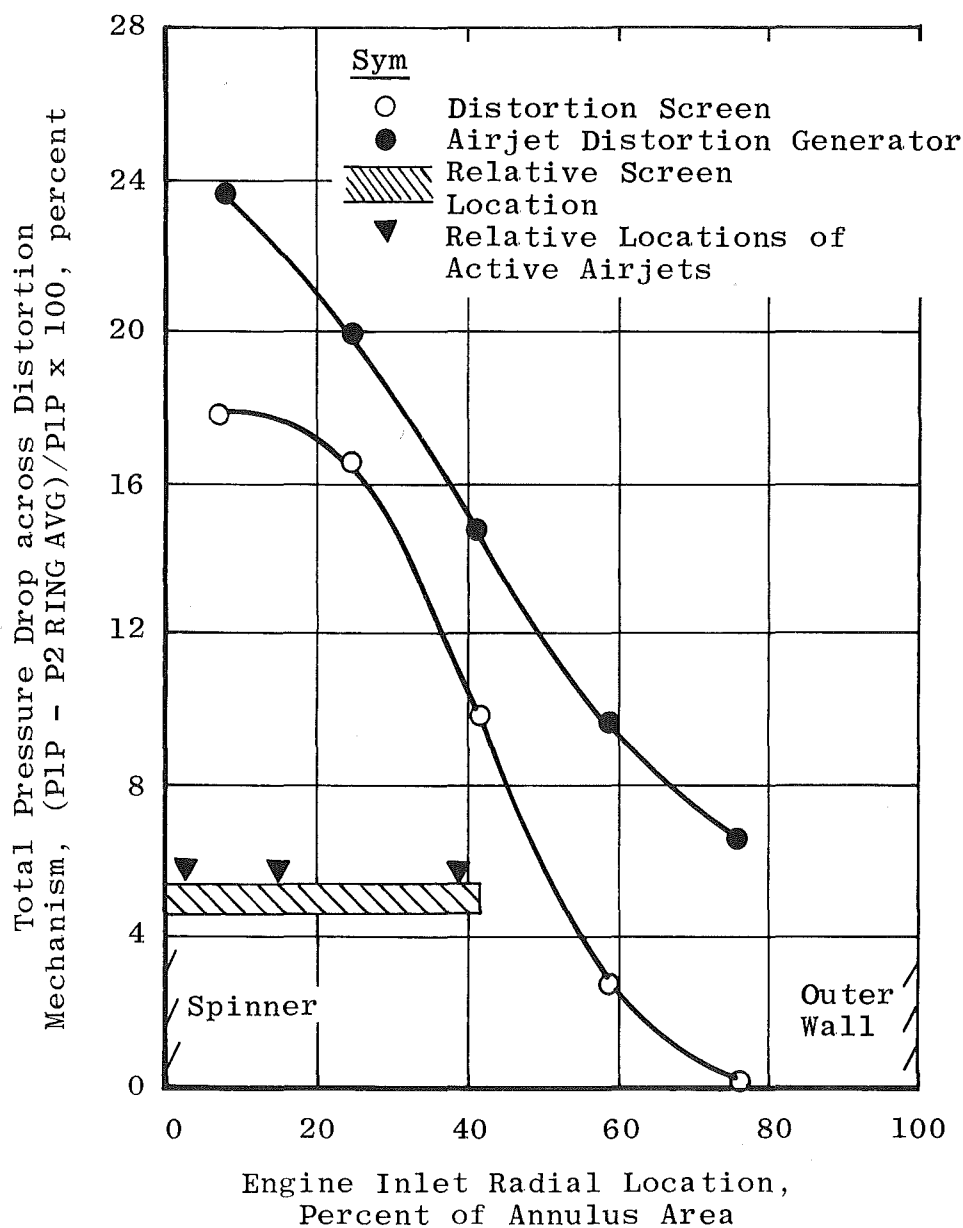


Figure 25. Comparison of radial distribution of total-pressure loss with screen and airjet distortion generator hub radial pattern at a corrected engine airflow of 200 lbm/sec.

Table 1. Posttest Estimates of Data Uncertainties

Parameter Designation	STEADY STATE ESTIMATED MEASUREMENT*								Range		Type of Measuring Device	Type of Recording Device	Method of System Calibration
	Precision Index (S)			Bias (B)		Uncertainty $\pm(B + t_{95}S)$							
	Percent of Reading	Unit of Measurement	Degree of Freedom	Percent of Reading	Unit of Measurement	Percent of Reading	Unit of Measurement	Amplitude	Frequency				
Venturi Inlet Static Pressure, PS00	+0.05	----	31	+0.15	----	+0.25	----	5 to 8 psia		Bonded Strain-Gage-Type Pressure Transducers	Automatic Multiple Pressure Scanning System onto Sequential Sampling, Millivolt-to-Digital Converter, and Magnetic Tape Storage Data Acquisition System	In-Place Application of Multiple Pressure Levels Measured with a Pressure-Measuring Device Calibrated in the Standards Laboratory	
Venturi Throat Static Pressure, PS1N	+0.05	----	31	+0.15	----	+0.25	----	3 to 4 psia					
Plenum Chamber Static Pressure, PS1P	+0.05	----	31	+0.15	----	+0.25	----	5 to 6 psia					
Inlet Duct Wall Static Pressure, PS03	+0.05	----	31	+0.15	----	+0.25	----	4 to 5 psia					
Fan Duct Inlet Total Pressure, P2.1C	+0.05	----	31	+0.15	----	+0.25	----	7 to 10 psia					
Fan Duct Total Pressure Downstream of Struts, P2.15C	+0.05	----	31	+0.15	----	+0.25	----	7 to 10 psia					
IP Compressor Inlet Total Pressure, P2.2	+0.05	----	31	+0.15	----	+0.25	----	7 to 10 psia					
IP Compressor Discharge Total Pressure, P2.3	+0.05	----	31	+0.15	----	+0.25	----	10 to 15 psia					
HP Compressor Discharge Total Pressure, P3	+0.1	----	31	+0.2	----	+0.4	----	50 to 80 psia					
Test Cell Pressure, PCELL	+0.05	----	31	+0.15	----	+0.25	----	2 to 3 psia					

*REFERENCE: Abernethy, R. B. and Thompson, J. W. Jr. "Handbook, Uncertainty in Gas Turbine Measurements." AEDC-TR-73-5 (AD755356), February 1973.

Table 1. Continued.

Parameter Designation	STEADY STATE ESTIMATED MEASUREMENT*							Range		Type of Measuring Device	Type of Recording Device	Method of System Calibration
	Precision Index (S)			Bias (B)		Uncertainty $\pm(B + t_{95S})$						
	Percent of Reading	Unit of Measurement	Degree of Freedom	Percent of Reading	Unit of Measurement	Percent of Reading	Unit of Measurement	Amplitude	Frequency			
Engine Inlet Total Pressure	± 0.1	----	31	± 0.2	----	± 0.4	----	5 to 6 psia		Bonded Strain-Gage-Type Pressure Transducers	Sequential Sampling, Millivolt-to-Digital Converter, and Magnetic Tape Storage Data Acquisition System	Resistance Shunt Based on the Standards Laboratory Determination of Transducer Applied Pressure versus Resistance Shunt Equivalent Pressure Relationship
Venturi Inlet Total Temperature, T00	----	$\pm 0.6^{\circ}\text{F}$	100	----	$\pm 0.9^{\circ}\text{F}$	----	$\pm 2.0^{\circ}\text{F}$	70 to 250°F		Copper-Constantan Temperature Transducers		Millivolt Substitution Based on the NBS Temperature versus Millivolt Tables
Plenum Chamber Total Temperature, T1P	----	$\pm 0.6^{\circ}\text{F}$	100	----	$\pm 0.9^{\circ}\text{F}$	----	$\pm 2.0^{\circ}\text{F}$	70 to 80°F				
Fan Duct Inlet Total Temperature, T2.15C	----	$\pm 0.6^{\circ}\text{F}$	100	----	$\pm 0.9^{\circ}\text{F}$	----	$\pm 2.0^{\circ}\text{F}$	150 to 300°F		Iron-Constantan Temperature Transducers		
IP Compressor Inlet Total Temperature, T2.2	----	$\pm 0.6^{\circ}\text{F}$	100	----	$\pm 0.9^{\circ}\text{F}$	----	$\pm 2.0^{\circ}\text{F}$	150 to 200°F				
IP Compressor Discharge Total Temperature, T2.3	----	$\pm 0.6^{\circ}\text{F}$	100	----	$\pm 0.9^{\circ}\text{F}$	----	$\pm 2.0^{\circ}\text{F}$	200 to 300°F		Chromel-Alumel Temperature Transducers		
HP Compressor Discharge Total Temperature, T3	----	$\pm 0.6^{\circ}\text{F}$	100	± 0.25	----	$\pm(1.2^{\circ}\text{F} + 0.25\%)$		600 to 900°F				
LP Turbine Discharge Total Temperature, T51	----	$\pm 0.6^{\circ}\text{F}$	100	± 0.25	----	$\pm(1.2^{\circ}\text{F} + 0.25\%)$		800 to 1000°F				

*REFERENCE:
NOTES:

Table 1. Concluded.

Parameter Designation	STEADY STATE ESTIMATED MEASUREMENT*							Range		Type of Measuring Device	Type of Recording Device	Method of System Calibration
	Precision Index (S)			Bias (B)		Uncertainty $\pm(B + t_{95}S)$						
	Percent of Reading	Unit of Measurement	Degree of Freedom	Percent of Reading	Unit of Measurement	Percent of Reading	Unit of Measurement	Amplitude	Frequency			
Low-Rotor Speed, NL	± 0.1	----	31	± 0.1	----	± 0.3	----	6000 to 8000rpm		Electromechanical Transducers	Frequency-to-Voltage Converter onto Sequential Sampling, Millivolt-to-Digital Converter, and Magnetic Tape Storage Data Acquisition System	Frequency Substitution Based on the Transducer and Transducer-to-Engine Rotor Coupling Characteristics
High-Rotor Speed, NH	± 0.1	----	31	± 0.1	----	± 0.3	----	10,800 to 11,700 rpm				
HPC Inlet Guide Vane Angle, IGV	----	$\pm 0.1^{\circ}$	31	----	$\pm 0.2^{\circ}$	----	$\pm 0.4^{\circ}$ Note.	0 to 35°		Rectilinear Potentiometer ↓	Sequential Sampling, Millivolt-to-Digital Converter, and Magnetic Tape Storage Data Acquisition System ↓	In-Place Measurement of Physical Dimensions versus Transducer Output ↓
7th Stage Bleed Lever Position, BVP	----	$\pm 0.2^{\circ}$	31	----	$\pm 0.5^{\circ}$	----	± 1 Note	0 to 100°				
Power Lever Angle, PLA	----	$\pm 0.3^{\circ}$	31	----	$\pm 0.5^{\circ}$	----	± 1 Note	40 to 65°				
Airjet Orifice Pressure, PASO	± 0.1	----	31	± 0.2	----	± 0.4	----	800 to 2000 psia		Bonded Strain-Gage-Type Pressure Transducers	Sequential Sampling, Millivolt-to-Digital Converter, and Magnetic Tape Storage Data Acquisition System ↓	Resistance Shunt Based on the Standards Laboratory Determination of Transducer Applied Pressure versus Resistance Shunt Equivalent Pressure Relationship
Airjet Orifice Temperature, TASO	----	$\pm 0.6^{\circ}\text{F}$	100	----	$\pm 0.9^{\circ}\text{F}$	----	$\pm 2.0^{\circ}\text{F}$	20 to 80°		Copper-Constantan Temperature Transducers		Millivolt Substitution Based on the NBS Temperature versus Millivolt Tables
Secondary Air Temperature, TAM	----	$\pm 0.6^{\circ}\text{F}$	100	----	$\pm 0.9^{\circ}\text{F}$	----	$\pm 2.0^{\circ}\text{F}$	70 to 250°				
Engine Inlet Total Temperature, T2	----	$\pm 0.6^{\circ}\text{F}$	100	----	$\pm 0.9^{\circ}\text{F}$	----	$\pm 2.0^{\circ}\text{F}$	70 to 250°				

*REFERENCE:

NOTE: Uncertainty Estimate Based on Experience with Systems Similar to Those Furnished by User.

Table 2. Summary of Steady-State Inlet Pattern Quality with Airjet Distortion Generator

Pattern	Nominal Corrected Engine Airflow, lbm/sec	$\frac{P2MAX - P2MIN}{P2AVG} \times 100, \%$		Overall Pattern Error, RMSE x 100, %
		Measured	Desired	
180 deg, one per revolution	200	21.7	21.5	1.7
	170	16.6	15.7	1.7
Tip radial	200	22.4	21.2	2.3
	170	18.4	15.9	0.7
Hub radial	200	21.9	22.3	2.1
	170	17.3	15.4	1.0
Composite	160	10.9	11.0	1.4
	180	11.9	11.0	1.0
	200	12.9	11.0	1.1
	240	15.3	11.0	1.3

APPENDIX A METHODS OF CALCULATION

General methods and equations employed to compute the steady-state and transient parameters presented are given below. Where applicable, arithmetic averages of the pressures and indicated temperatures were used.

SPECIFIC HEATS

The specific heat at a constant pressure was computed from the empirical equation:

$$CP = \frac{(a_1 + b_1 T + c_1 T^2) + (a_2 + b_2 T + c_2 T^2) FA}{1 + FA}$$

where a_1 , b_1 , and c_1 are constants based on the specific heats of the constituents of air; a_2 , b_2 , and c_2 are the constants based on a fuel hydrogen-carbon ratio of 0.16 and the specific heats of water vapor, oxygen, and carbon dioxide, and FA is the fuel-air ratio. The equation was derived for the two temperature ranges shown below:

Temperature Range, °R	a_1	b_1	c_1	a_2	b_2	c_2
400 to 1,700	0.2318	0.104×10^{-4}	0.7166×10^{-8}	0.2655	3.7265×10^{-4}	-6.6353×10^{-8}
1,701 to 4,500	0.2214	0.3521×10^{-4}	-0.3376×10^{-8}	0.3397	2.7182×10^{-4}	-2.9044×10^{-8}

RATIO OF SPECIFIC HEATS

The ratio of specific heats was calculated from the expression:

$$\gamma = \frac{CP}{CP - R/J}$$

For a fuel-air mixture, the gas constant was expressed as

$$R = \frac{53.34 + 52.863 FA}{1 + FA}$$

TOTAL TEMPERATURE

Gas temperatures were measured using Chromel-Alumel (CA), Iron-Constantan (IC), and copper-constantan (CC) thermocouples. No recovery factor corrections were applied to the internal engine thermocouples.

Venturi Inlet

The venturi inlet thermocouples were mounted on a straightening grid located 85 in. upstream of the venturi inlet in the venturi plenum chamber. Gas temperature (T00) was defined as equal to the indicated temperature.

Engine Inlet Temperature

Engine inlet temperature (T2) was determined from the grid temperatures measured in the test cell plenum chamber and the relationship to the engine inlet temperature established during a prior test program (Fig. A-1) for the engine test. Measurements from CA thermocouples were used to define inlet temperature during the simulator test.

MACH NUMBER

For stations where both the static and total pressure were measured, the Mach number was obtained from the equation:

$$M = \sqrt{\frac{2}{\gamma - 1} \left[\left(\frac{P}{P_S} \right)^{\frac{\gamma-1}{\gamma}} - 1 \right]}$$

For stations where the static pressure was not measured, Mach number was obtained from an iterative solution of the relationship:

$$\frac{W \sqrt{T}}{P A} = \frac{\sqrt{\gamma} M}{\sqrt{\frac{R}{g_c}} \left(1 + \frac{\gamma - 1}{2} M^2 \right)^{\frac{\gamma+1}{2(\gamma-1)}}}$$

VELOCITY

Velocity was determined from the relation:

$$V = \sqrt{\frac{2\gamma g_c R T}{\gamma - 1} \left[1 - \left(\frac{P_S}{P} \right)^{\frac{\gamma-1}{\gamma}} \right]}$$

GAS FLOW

Airflow at station 1N (venturi throat) was calculated from the following equation for critical venturi flow as follows:

$$WA_{1N} = P_{S00} \times A_{1N} \times C_{F1N} \times C_T \left(\frac{2}{\gamma + 1} \right)^{\frac{\gamma+1}{2(\gamma-1)}} \sqrt{\frac{\gamma g_c}{R T_{00}}}$$

When the venturi was unchoked, airflow was calculated using the relation:

$$WA_{1N} = \sqrt{\frac{2\gamma g_c}{R(\gamma - 1)}} \frac{P_{S1N} \times A_{1N} \times C_{F1N} \times C_T \sqrt{1 - \left(\frac{P_{S1N}}{P_{S00}} \right)^{\frac{\gamma-1}{\gamma}}}}{\sqrt{T_{00}} \left(\frac{P_{S1N}}{P_{S00}} \right)^{\frac{\gamma-1}{\gamma}}}$$

where C_T is the thermal growth correction coefficient for the venturi throat area (A_{1N}) and where C_{F1N} is an empirically determined flow coefficient based on the venturi wall curvature, area ratio, and boundary-layer development (Refs. 8 and 9). The flow coefficient was evaluated and expressed as a function of venturi throat Mach number (M_{1N}) and Reynolds number based on throat diameter (RE_{1N}) as follows:

For a choked venturi:

$$C_{F1N} = 0.9843 + 0.0017 \log RE_{1N}$$

For an unchoked venturi:

$$CF1N = 0.9843 + 0.0017 \log RE1N - 0.0267 (1 - M1N)$$

The airflow to the airjet system (WAS) was measured using a standard ASME sharp-edged orifice with flange taps and calculated as follows:

$$W_s = 6.3018 \times C_f \times f \times d^2 \times C_t \times Y \left[\frac{P_u (P_u - P_d)}{R T} \right]^{1/2}$$

where

6.3018 = a conversion constant

C_f = a flow coefficient

f = the velocity approach factor = $\frac{1}{\sqrt{1 - B^4}}$

$B = \frac{\text{throat diameter}}{\text{pipe diameter}}$

d = throat diameter

C_t = thermal expansion coefficient

Y = adiabatic expansion factor
 $= 1 - \frac{P_u - P_d}{\gamma P_u} (0.41 + 0.35B^4)$

P_u = static pressure upstream of orifice

P_d = static pressure downstream of orifice

ENGINE INLET AIRFLOW

Engine inlet airflow (WA2) is the sum of venturi and airjet airflow

$$WA2 = WA1N + WAS$$

Air or gas flows at the other stations were obtained as follows:

WA22 = Obtained by utilizing a high-pressure turbine flow parameter discussed in the following section

$$WA21 = WA2 - WA22$$

$$WA23 = WA22$$

$$WA24 = WA23$$

$$WA3 = WA24 - WBHPC$$

$$WG4 = WA3 + WIB + WFE$$

$$WG41 = WG4 + WCHPT$$

$$WG42 = WG41$$

$$WG50 = WG42 + WCLPT - WCLP$$

$$WG6 = WA2 + WIB - WLHPC - WLD - WCLP + WFE$$

The inbleed airflow (WIB) was calculated from the previously defined equation for a standard ASME sharp-edged orifice.

The overboard low-pressure turbine cooling flow (WCLP) was determined by an instrumented measurement section of straight pipe from the relation

$$WCLP = \sqrt{\frac{2\gamma g_c}{R(\gamma - 1)}} \frac{PSCLP \times ACLP \sqrt{1 - \left(\frac{PSCLP}{PCLP}\right)^{\frac{\gamma-1}{\gamma}}}}{\sqrt{TCLP} \left(\frac{PSCLP}{PCLP}\right)^{\frac{\gamma-1}{\gamma}}}$$

The following bleed and leakage flows were calculated using constants furnished by the engine manufacturer as follows:

$$WBHPC = 0.07712 (WA3 + WIB)$$

$$WCHPT = 0.0547 WA24$$

$$WCLPT = 0.0070 WA24$$

$$WLHPC = 0.0020 WA24$$

$$WLD = 0.0090 WA24$$

INTERMEDIATE-PRESSURE COMPRESSOR AIRFLOW

Airflow to the intermediate-pressure compressor (WA22) was calculated based on energy-continuity relationships and

the assumption of choked flow at the high-pressure turbine first-stage nozzle vane, station 4. The turbine flow parameter was determined from the relationship:

$$\frac{WG4 \sqrt{T4X}}{P4X} = \frac{A4 \times CF4 \sqrt{\gamma} M4}{\sqrt{\frac{R}{gc}} \left(1 + \frac{\gamma - 1}{2} (M4)^2 \right)^{\frac{\gamma+1}{2(\gamma-1)}}}$$

where

$$\gamma = \gamma_4$$

By assuming choked flow at the high-pressure turbine (first-stage nozzle vane, station 4), the following relationship results:

$$\frac{WG4 \sqrt{T4X}}{P4X} = \frac{A4 \times CF4 \sqrt{\gamma}}{\sqrt{\frac{R}{gc}} \left(1 + \frac{\gamma - 1}{2} \right)^{\frac{\gamma+1}{2(\gamma-1)}}}$$

where $A4 \times CF4 = 46.85 \text{ in.}^2$ was determined by Detroit Diesel Allison Division of General Motors from vane airflow calibrations and $P4X$ and $T4X$ were determined from iterative solutions of the equations presented in the following sections of high-pressure turbine inlet total-pressure and turbine inlet temperature, respectively.

The intermediate-pressure compressor airflow, $WA22$, is then determined from $WG4$ and the gas flow relationships.

HIGH-PRESSURE TURBINE INLET TOTAL PRESSURE

High-pressure turbine inlet total pressure was determined from an empirical burner pressure loss parameter supplied by the engine manufacturer as follows:

$$P4X = P3 \left[1 - 20.5 \left(\frac{WA4 \sqrt{T3}}{P3 \times ABURNER} \right) \right]^2$$

where $ABURNER = 315.5 \text{ in.}^2$.

HIGH-PRESSURE TURBINE INLET ENTHALPY

The enthalpy at station 4 was obtained as a function of burner inlet conditions and the assumed burner efficiency as follows:

$$H4X = \frac{WA3 \times H3 + WIB \times HIB + ETA3M \times WFE \times LHV + WFE \left[59.62 + \int_{540^{\circ}R}^T CP_{fuel} \times dT \right]}{WG4}$$

LHV is the lower heating value of the fuel and the quantity 59.62 (Btu/lbm) accounts for the difference between the enthalpy of carbon dioxide and water vapor formed during combustion and enthalpy of the oxygen removed from the air by their formation in the temperature range from 400°R (base of the enthalpy equation) to 540°R (reference temperature for determination of LHV). The assumed burner efficiency (ETA3M) was obtained from the engine manufacturer (Fig. A-2).

HIGH-PRESSURE TURBINE INLET TEMPERATURE

The temperature at station 4 was obtained from an iteration of the equation:

$$\int_{400^{\circ}R}^{T4X} CP \times dT = H4X$$

BYPASS RATIO

The bypass ratio was calculated from the following relationship:

$$BPR = \frac{W2 - WA22}{WA22}$$

where WA2 is the total engine airflow, and WA22 is the airflow to the intermediate-pressure compressor.

FAN DISCHARGE TOTAL PRESSURE

The fan discharge total pressure was determined by mass weighting the measurement at the fan discharge as follows:

$$PAVLPCEX = \frac{BPR \times P21 + P22}{1 + BPR}$$

HIGH-PRESSURE COMPRESSOR INLET TOTAL PRESSURE

High-pressure compressor inlet total pressure was determined from an empirical inter-compressor duct pressure loss parameter supplied by the engine manufacturer as follows:

$$P_{24X} = P_{23} \left[1 - 0.00000605 \left(\frac{WA_4}{A_{23}} \sqrt{\frac{T_{23}}{518.7}} \frac{14.696}{P_{23}} \right)^2 \right]$$

where $A_{23} = 51.41 \text{ in.}^2$.

REYNOLDS NUMBER INDEX

Reynolds number index was obtained from the relationship:

$$REI_2 = \frac{\Delta T_2}{\phi \quad \theta_2}$$

where

$$\phi = \frac{718.2 (\theta_2)^{3/2}}{T_2 + 199.5}$$

COMPRESSOR SURGE MARGIN

Fan and high-pressure compressor surge margin was based on total-pressure ratio and calculated as follows:

Fan

$$\left[\frac{\left(\frac{PLPCEX}{P_2} \right)_{SURGE} - \left(\frac{PLPCEX}{P_2} \right)_{NOL}}{\left(\frac{PLPCEX}{P_2} \right)_{NOL}} \right]_{WA2R2=K} \quad \times 100, \text{ percent}$$

High-Pressure Compressor

$$\left[\frac{\left(\frac{P_3}{P_{23}} \right)_{\text{SURGE}} - \left(\frac{P_3}{P_{23}} \right)_{\text{NOL}}}{\left(\frac{P_3}{P_{23}} \right)_{\text{NOL}}} \right] \times 100, \text{ percent}$$

WA24R24=K

INLET PATTERN ERROR

The inlet pattern error (RMSE) was calculated using the following equation:

$$\text{RMSE} = \sqrt{\frac{\sum_{I=1}^N \left[\frac{\left(\frac{P_I}{P_2} \right)_{\text{MEASURED}}}{\left(\frac{P_I}{P_2} \right)_{\text{DESIRED}}} - 1 \right]^2}{N}} \times 100, \text{ percent}$$

where P_I/P_2 = ratio of local to average total pressure

N = number of total-pressure probes

INLET TOTAL-PRESSURE DISTORTION

The distortion at the engine inlet $P_2\text{DIST}$ was defined as follows:

$$P_2\text{DIST} = \frac{P_{2\text{MAX}} - P_{2\text{MIN}}}{P_2} \times 100, \text{ percent}$$

POWER SPECTRAL DENSITY FUNCTION

The power spectral density (PSD) function was computed by an electronic analog wave analyzer and presented graphically as a function of frequency. The PSD function of a stationary signal is mathematically defined as

$$\text{PSD} = \lim_{T \rightarrow \infty} \lim_{\Delta f \rightarrow 0} \frac{1}{(\Delta f)T} \int_0^T Y^2(t, f, \Delta f) dt$$

where T is the averaging time of the data, f is the bandwidth of the electrical filter used, and Y(t,f,Δf) is the instantaneous value of the data waveform at time t within the bandwidth Δf. The square root of the total area under the PSD curve is equal to the total root-mean-square (RMS) value of the signal. The PSD function indicates the magnitude, the energy distribution with frequency, and the existence of any discrete frequency components of the total input signal. The PSD functions presented in this report were normalized by the steady-state total pressure as follows:

$$\frac{\text{PSD}}{(p)^2} = \frac{\frac{\Delta p}{p}^2}{\text{Hz}}$$

The PSD functions presented herein were generally obtained using a 10-Hz electrical bandwidth filter, a 1-sec averaging time, and a 10.0-sec data sample.

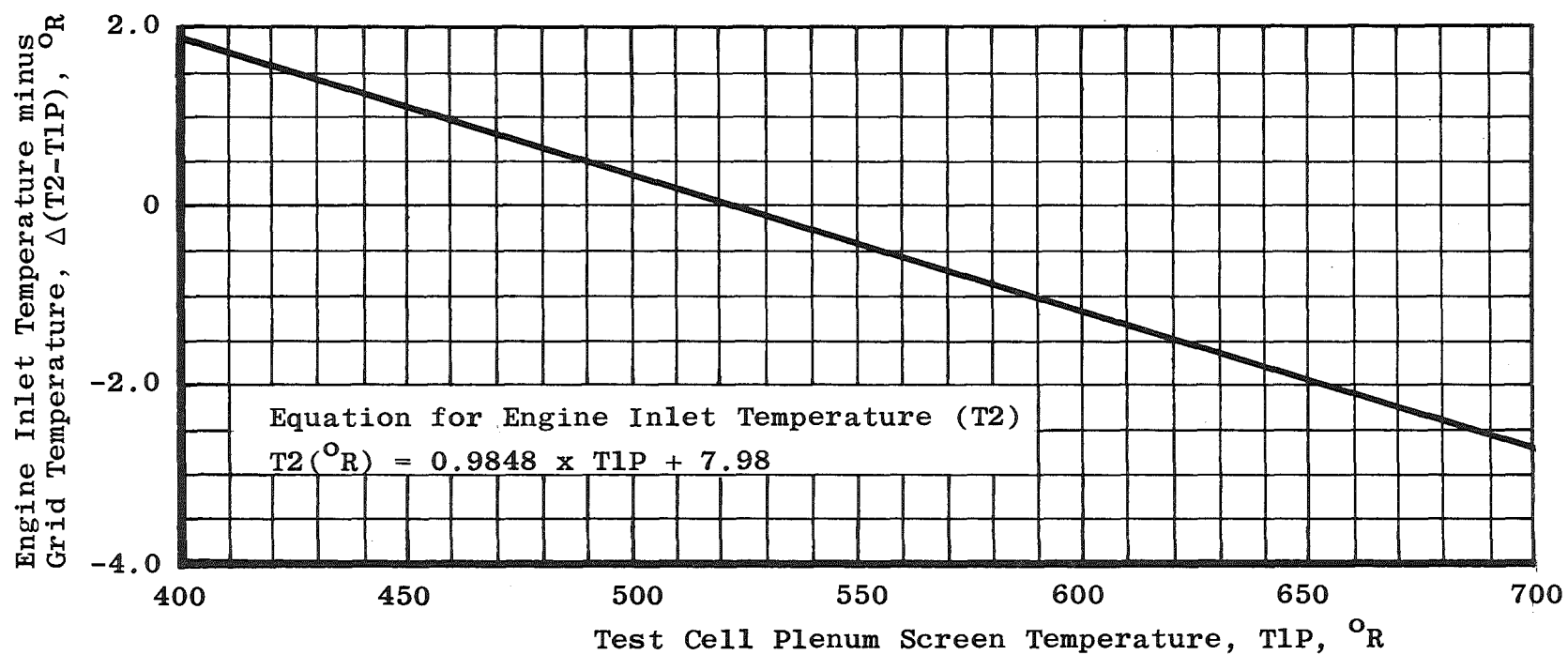


Figure A-1. Engine inlet air temperature correlation to test cell plenum grid temperature.

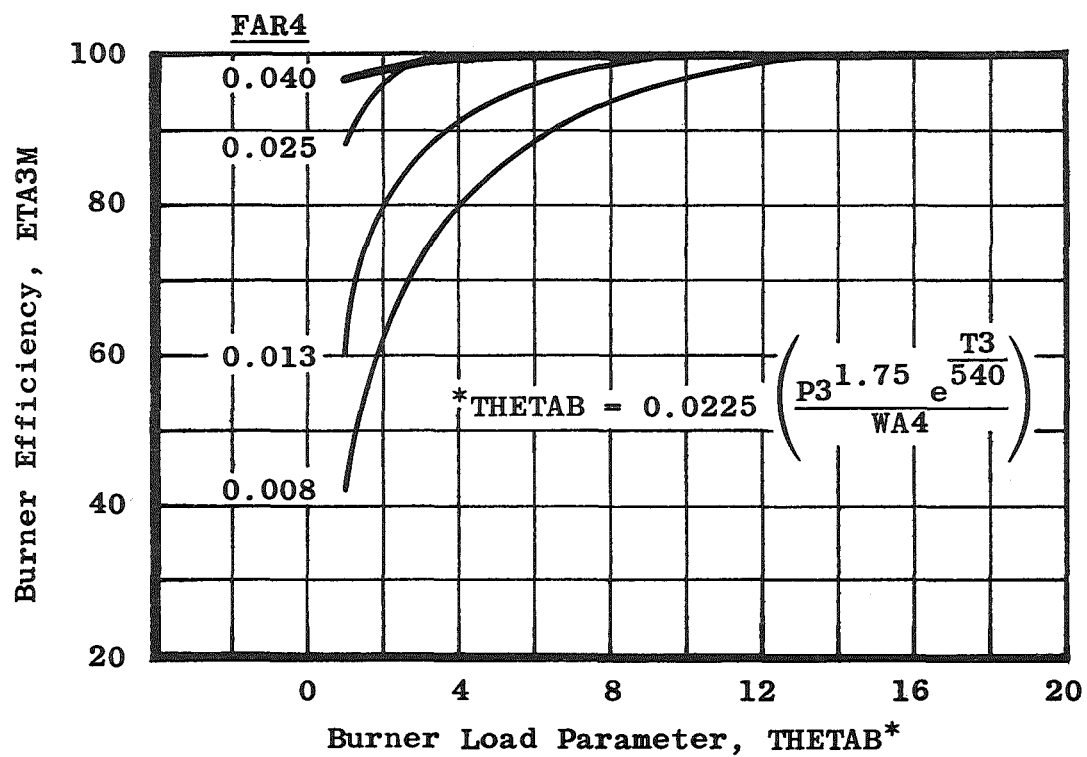


Figure A-2. Burner efficiency as a function of burner load parameter.

NOMENCLATURE

A	Area, in. ² ; air
AJDG	Airjet Distortion Generator
ALT	Altitude, ft
APLUG	Nozzle plug position, inches from fully retarded
A8	Exhaust nozzle exit area, in. ²
BPR	Bypass ratio
BVP	Bleed valve position, percent open
DP	Pressure difference, psi
gc	Dimensional constant, 32.174 lbm-ft/lbf-sec ²
H	Enthalpy, Btu/lbm
IGV	High-pressure compressor inlet guide vane position, deg
M	Mach number
NH	High-pressure rotor speed, rpm
NL	Low-pressure rotor speed, rpm
NR	Inlet duct total-pressure recovery ratio
P	Total pressure, psia
PC	Percent
PLA	Power lever angle, deg
PS	Static pressure, psia
PSO	Free-stream ambient pressure, test cell pressure, psia
R	Gas constant for air, 53.34 ft-lbf/lbm-°F
RE	Reynolds number
REI	Reynolds number index
T	Total temperature, °F, °R
TS	Static temperature, °F, °R
TSO	Free-stream ambient temperature, °F, °R
V	Velocity, ft/sec
W	Mass flow rate, lbm/sec, lbm/hr
γ	Ratio of specific heats

POSTSCRIPTS

SO	Equivalent free-stream ambient conditions
1N,1,2,etc.	Instrumentation stations
A	Air, averaged
AVG	Averaged
C	Fan duct
CC	Close coupled
DIST	Distortion
FAN,LPC	Low-pressure compressor
G	Gas
HUB	Fan hub
HPC	High-pressure compressor
HR	High-response pressure transducer
IB	Inbleed
K	Constant
M	Mixed, manifolded
Q	Divided by
R2,R3,etc.	Corrected to Station 2, 3, 35c
TIP	Fan tip
X	Calculated
7STG	Seventh-stage of high-pressure compressor

STATIONS

00	Airflow-measuring venturi inlet
1N	Airflow-measuring venturi throat
1P	Test cell plenum
03	Engine inlet duct upstream of lab seal
LS	Lab seal cavity
05,08	Engine inlet duct downstream of lab seal
1	Instrumented engine inlet extension
2	Engine inlet
2.1C, (21C)	Fan duct entrance
2.2, (22)	Intermediate compressor inlet

2.15, (215C)	Fan duct entrance downstream of inlet strut
2.3, (23)	Intermediate compressor outlet
2.4, (24)	High-pressure compressor inlet
2.5, (25)	Seventh-stage high-pressure compressor
3	High-pressure compressor outlet